Geophysical Journal International

Geophys. J. Int. (2022) **231,** 2102–2126
Advance Access publication 2022 August 17
GJI Geodynamics and Tectonics

https://doi.org/10.1093/gji/ggac316

Active tectonics and fault evolution in the Western Balkans

N. D'Agostino [1], A. Copley,[2] J. Jackson,[2] R. Koçi,[3] A. Hajrullai,[3] L. Duni[3] and N. Kuka[3]

[1] *Osservatorio Nazionale Terremoti, Istituto Nazionale Geofisica e Vulcanologia, 00153 Roma, Italy. E-mail: nicola.dagostino@ingv.it*
[2] *Bullard Laboratories, University of Cambridge, Cambridge, CB2 3EQ, UK*
[3] *Department of Seismology, Institute of Geosciences, Energy, Water and Environment,1024 Tirana, Albania*

Accepted 2022 August 12. Received 2022 July 22; in original form 2022 April 29

SUMMARY

The western Balkans occupy a region influenced by two major active tectonic processes: the collision between the Adriatic Region and the Dinarides in the west, and the extension of the Aegean Region and its surroundings as they move towards the Hellenic Trench. An understanding of the kinematics and dynamics of the western Balkans has significance for our understanding of continental tectonics in general, and is the object of this paper. The region is rich in observational data, with many well-studied earthquakes, good geodetic coverage by GNSS (Global Navigation Satellite System) and abundant exposure of active faulting and its associated geomorphology, especially within the Mesozoic carbonates that cover large sectors of the extensional areas. We first use such observations to establish the regional kinematic patterns, by which we mean a clarification of how active faulting achieves the motions observed in the deforming velocity field obtained from GNSS measurements. We then use geomorphological observations on the evolution of drainage systems to establish how kinematic and faulting patterns have changed and migrated during the Late Neogene-Quaternary. The kinematics, and its evolution, can then be used to infer characteristics of the dynamics, by which we mean the origin and effect of the forces that control the overall deformation. The principal influences are: (i) the distribution and evolution of gravitational potential energy (GPE) contrasts arising from crustal thickness variations and elevation, in particular the growth of topography by shortening in the Albanides–Hellenides mountain ranges and the high elevation of mainland Greece relative to the Mediterranean seafloor and (ii) the ability of the boundaries of the region, along the Adriatic coast and in the Hellenic Trench, to support the forces arising from those GPE contrasts. The evolution in space and time indicates an interaction between the anisotropic strength fabric of the upper crust associated with faulting, and the more distributed and smoother patterns of flow that are likely to characterize the ductile deformation of the lower, aseismic part of the lithosphere—both of which influence the deformation on the scale of 100–200 km. The persistent argument about whether continental deformation is best described by a continuum or by rigid-block motions is largely a matter of scale and particular location: both are influential in establishing the patterns we see.

Key words: Seismicity and tectonics; Continental neotectonics; Dynamics and mechanics of faulting; Tectonics and landscape evolution.

1 INTRODUCTION

An adequate description of large-scale distributed continental deformation requires knowledge of both the overall deforming velocity field and how it is achieved by active faulting. The two aspects are closely related, since the azimuthal directions of no-length-change in the velocity field, which are uniquely determined by the strain-rate tensor, are the strike directions of organized faulting that can accommodate the motion (Jackson *et al.* 1992; Haines & Holt 1993). However, such a picture is only instantaneous, accounting for the motions at the present time. In many places it is known, from palaeomagnetism or from the discordance between the velocities and slip-vector directions on the faults themselves, that substantial rotations of fault blocks occur, especially about vertical axes. In such cases the relationship between the velocity field and the faulting must be unstable: if the faults rotate, then the velocity field must itself change to keep the no-length-change directions parallel to the faulting; alternatively, new fault systems could form to accommodate the unchanging velocity field while older faults rotate out of a suitable orientation. The relationship between the instantaneous

(present-day) deformation and the finite deformation over a period of time, which produces topography and the geological record, can therefore be subtle, and to be understood clearly needs information about the evolution through time. That is the focus and purpose of this paper. We aim to show that, with sufficient observations of earthquake focal mechanisms, faulting in the field and GPS measurements, a robust and coherent picture of the regional kinematics can be obtained, which can then, in turn, clarify our understanding of the underlying dynamic processes. Key questions include: how does active faulting relate to the instantaneous velocity field? How does the active faulting change spatially? Is there evidence for it also changing with time and what are the dynamic implications?

Over the past 50 yr the Western Balkans, central Greece and the Aegean Sea have been influential in advancing our understanding of distributed deformation and faulting, and their link to lithosphere dynamics (e.g. McKenzie 1978; Le Pichon 1982; England *et al.* 2016). A general feature of the region is the motion of the crust from regions of high to low gravitational potential energy (GPE) under the effect of buoyancy forces and strength heterogeneities in the lithosphere (e.g. McKenzie 1978; Copley *et al.* 2009; Métois *et al.* 2015). The upper, brittle part of the lithosphere accommodates this deformation by discontinuous faulting and large rotations about vertical axes (Kissel *et al.* 1985; Goldsworthy *et al.* 2002). Previous studies described both spatial (e.g. Goldsworthy *et al.* 2002; Howell *et al.* 2017) and temporal (e.g. Pavlides & Mountrakis 1987; Mercier *et al.* 1989; Caputo & Pavlides 1993; Jackson 1999; Mattei *et al.* 2004) changes in the directions of crustal extension in the broader Aegean Region. Changes in the orientation of active faulting may arise from a change in the regional velocity field, and the need to accommodate it by discontinuous faulting, or by rotations about vertical axes, which bring rotated faults in unfavourable directions to accommodate the regional velocity field (Jackson 1999). Thus, the change in fault orientation with time has been interpreted as either a change in the regional stress field (e.g Mercier *et al.* 1989) or to block rotations about a vertical axis (e.g. McKenzie & Jackson 1983; Goldsworthy *et al.* 2002), both of which have implications for the dynamics of the deformation.

We will discuss the deformation in the western Balkans and northern Greece (Fig. 1), synthesizing new earthquake source inversions and field observations with published earthquake-source models, GPS velocities, Late Neogene-Quaternary geology and geomorphology, to develop a consistent kinematic picture. We first describe the organization of faulting, and its spatial and temporal changes, and then its relationship with the forces driving the deformation in this region. We conclude that the evolution of topography and crustal thickness contrasts in response to the deformation within the broader region are likely to be the sources of the rapid spatial and temporal variations of the organized faulting. Our observations indicate that large-scale GPE contrasts and also local fault kinematics both exert important controls on the distribution of deformation in space and time, with implications for the persistent debate regarding the relative merits of continuum and micro-plate models of continental tectonics.

2 METHODS

2.1 Earthquake focal mechanisms, slip vectors and depths

Earthquake focal mechanisms (Fig. 2a) and well-constrained centroid depths (Fig. 2b) are updated from Copley *et al.* (2009), and obtained with the same methods described in that paper, in the following hierarchy:

(1) Earthquakes whose teleseismic long-period *P* and *SH* waveforms have been modelled, using the Zwick *et al.* (1995) MT5 version of the inversion algorithm of McCaffrey & Abers (1988) and McCaffrey *et al.* (1991), imposing double-couple solutions, to refine both focal mechanisms and centroid depths. Long-period waveforms are insensitive to small-scale heterogeneity in the source region velocity structure (Taymaz *et al.* 1990), so we used a simple 1-D crustal velocity model with $V_p = 6.5$ km s^{-1}, $V_s = 3.7$ km s^{-1} and density 2800 kg m^{-3} in all the moment-tensor solutions. The uncertainty in the depths, arising from the velocity model and waveform fits, is about ±3 km (Taymaz *et al.* 1990). The Supporting Information contains the results of the original inversions of 13 earthquakes that occurred in 1990–2021 in the southwestern Balkans with *P* and *SH* observed and modelled waveforms (Table S1 and Figs S1–S13). Table S2 (Supporting Information) contains source parameters for other earthquakes obtained in the same way, using MT5, by previous studies.
(2) 'Best-double-couple' versions of the centroid moment tensors from the gCMT catalogue (www.globalcmt.org), for earthquakes with more than 70 per cent double-couple component as defined in Jackson *et al.* (2002), that have not been modelled with the MT5 algorithm (Table S3, Supporting Information). The gCMT centroid depths for the relatively shallow earthquakes of interest here are rarely well determined, and are not used in this paper, which only uses the (more accurate) gCMT fault-plane solutions.
(3) Earthquakes, generally in the magnitude (M_w) range 5.0–5.3 and usually with gCMT solutions, that are too small for long-period MT5 modelling, but whose teleseismic broad-band vertical-component seismograms can be modelled with the WKBJ3 program of Chapman (1978) to identify *pP* and *sP*, and thereby determine depth (see Copley *et al.* 2009, for details of the method).
(4) Some teleseismic first-motion fault-plane solutions (Table S4, Supporting Information) from McKenzie (1972) or Anderson & Jackson (1987) for earthquakes that occurred before or were omitted from the gCMT catalogue (see Copley *et al.* 2009).
(5) Selected focal mechanisms from regional CMT solutions (Table S5, Supporting Information) obtained from the MED-NET network, in a few places where nothing else is available (http://rcmt2.bo.ingv.it).

Azimuths of slip vectors (Fig. 3) have been chosen on the basis of field observations of surface faulting, or earthquake focal mechanisms. We only include slip vectors from focal mechanisms when the difference between the slip vectors of the two auxiliary planes is less than 20°, and take the average direction. For earthquakes along the contractional Albanides–Hellenides coastal belt we systematically selected the slip vector corresponding to the low-angle east-dipping nodal plane, as dip-slip faulting on the other, near-vertical, nodal plane is geologically unlikely.

2.2 GPS velocity field and strain rate

We used an homogeneously-processed GPS velocity field of the Balkans area based on data from continuous GNSS stations (D'Agostino *et al.* 2020). In central Greece we integrate the velocity field with 30 horizontal velocities taken from the velocity data set of permanent stations in Briole *et al.* (2021). Before station integration, the velocity field of Briole *et al.* (2021) was rotated into

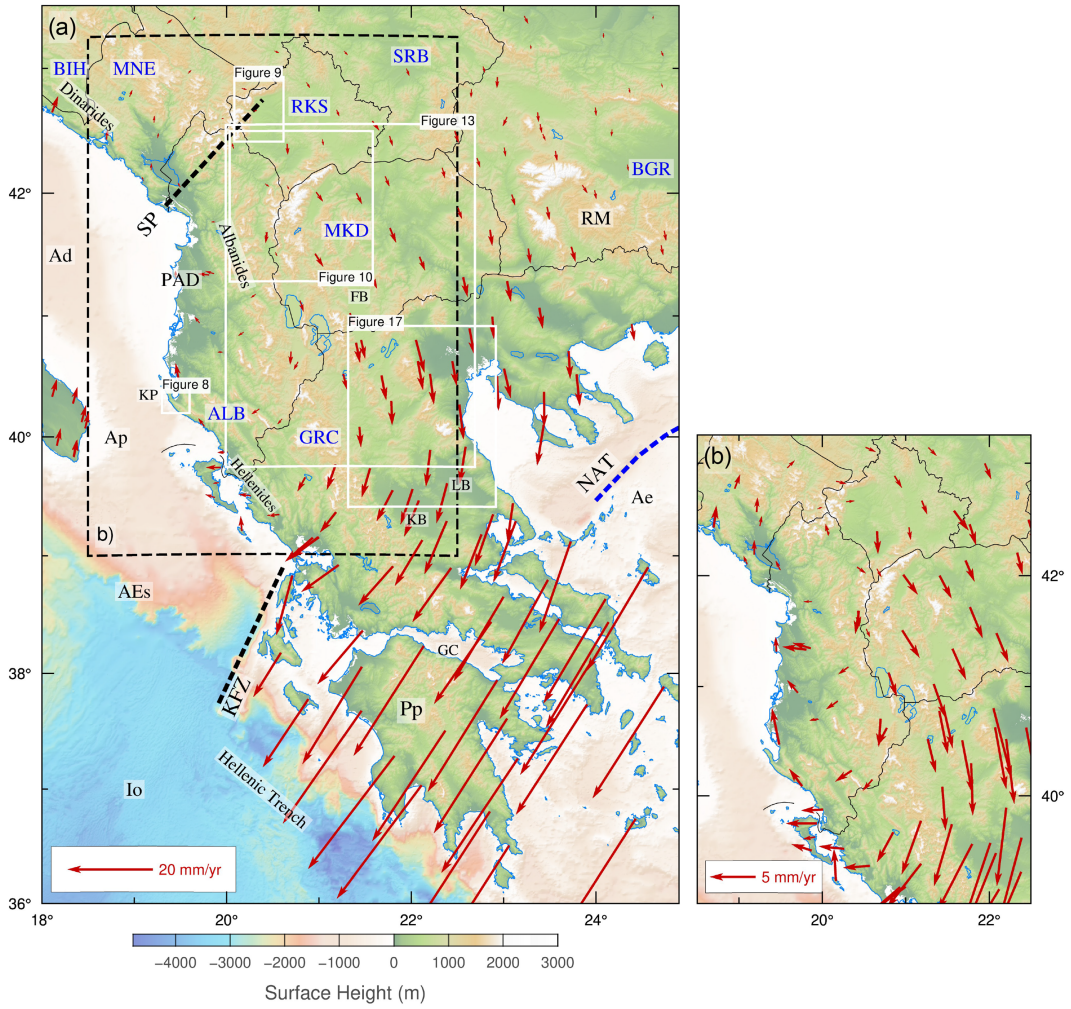

Figure 1. SRTM15+ topography (Tozer *et al.* 2019) and GPS velocities relative to Eurasia. (a) Selected representative velocities from D'Agostino *et al.* (2020) and Briole *et al.* (2021) rotated in the Eurasian reference frame of D'Agostino *et al.* (2020, see the text for details) and main physiographic features of the southwestern Balkans and western Greece. Ad, Adria; Ae, Aegean Sea; AEs, Apulia Escarpment; Ap, Apulia; FB, Florina Basin; GC, Gulf of Corinth; Io, Ionian Sea; KB, Karditsa Basin; KP, Karaborun Peninsula; KFZ, Kephalonia Fault Zone;LB, Larissa Basin; NAT, Northern Aegean Trough; Pp, Peloponnese; PAD, Peri-Adriatic Depression; RM, Rhodopes Massif;SP, Scutari-Pec (Shkoder-Peja) transverse zone. Country codes: ALB, Albania; BIH, Bosnia Herzegovina; BGR, Bulgaria; GRC, Greece; MKD, Northern Macedonia; MNE, Montenegro; RKS, Kossovo and SRB, Serbia. (b) Enlarged view of the velocity field.

the Eurasian reference frame of D'Agostino *et al.* (2020) by applying a rotation estimated by minimizing the difference of horizontal velocities at common stations. The GPS velocities were then used to estimate the strain-rate field (Fig. 4) employing the code VISR by Shen *et al.* (2015) through a weighted least-squares inversion procedure that minimizes the GPS velocity post-fit residuals using a net reweighting threshold $W_t = 12$. The effect of changing this parameter has been investigated for the same area by D'Agostino *et al.* (2020) and is shown in their Fig. 5. In order to investigate the relationships between the regional velocity field and faulting directions that accommodate it, we also determine no-length-change orientations from our strain-rate field. Because faulting can cause no change in length between points joined by a line parallel to the faults, these no-length-change orientations correspond to the strikes of faults that can accommodate the strain-rate field. In any continuous velocity field where the shear-strain rate exceeds the dilatation rate there are, in general, two directions in which a line joining two points does not change in length (Holt & Haines 1993). Where this requirement is satisfied, the two directions show possible orientations of faults that can accommodate the strain-rate field by uniform slip on faults of a single strike. Where this requirement is not satisfied, the velocity field cannot be accommodated by uniform slip on a parallel system of faults, and more than one fault orientation must be involved, as for example in SW Turkey (Howell *et al.* 2017). The directions of zero-length-change in the velocity field, measured anticlockwise from the x axis, in terms of the elements of the strain rate tensor, are:

$$\tan\theta_f = \frac{-\dot{\epsilon}_{xy} \pm \sqrt{\dot{\epsilon}_{xy}^2 - \dot{\epsilon}_{xx}\dot{\epsilon}_{yy}}}{\dot{\epsilon}_{yy}} \tag{1}$$

where the x-direction is east and the y-direction is north. This result is correct only if

$$\dot{\epsilon}_{xy}^2 \geq \dot{\epsilon}_{xx}\dot{\epsilon}_{yy} \tag{2}$$

which is equivalent to requiring that the principal horizontal strain rates have opposite signs, or that one is zero (Holt & Haines 1993). Where condition (2) is satisfied the velocity field can be accommodated by faulting with either of two strikes, corresponding to the two azimuths of the zero-length-changes in Fig. 4(b).

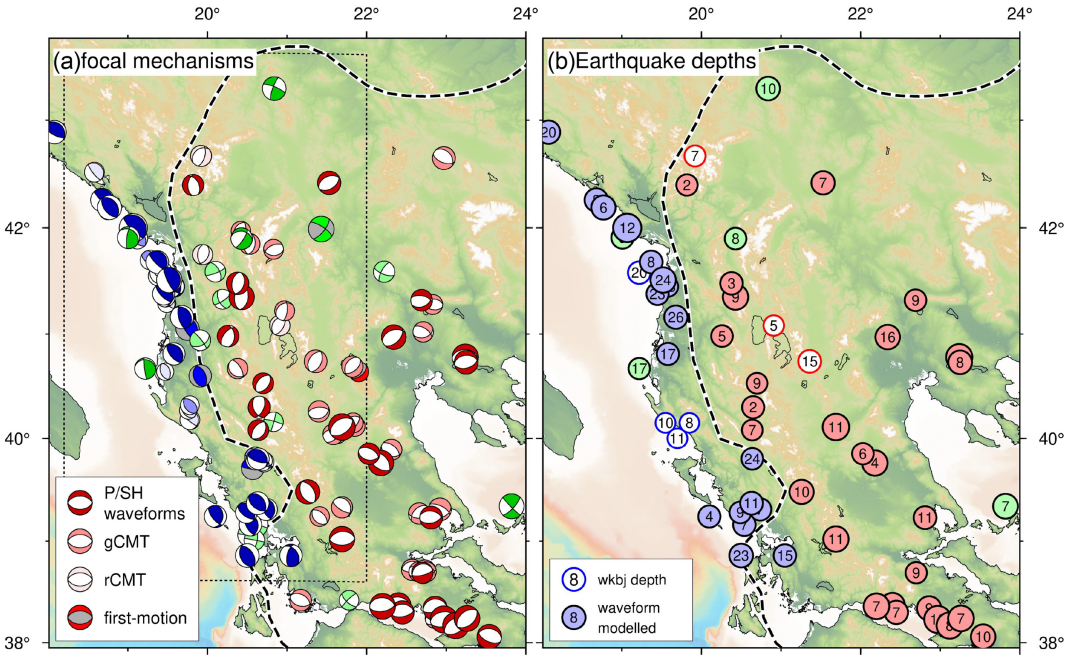

Figure 2. Seismicity of the western Balkans. (a) Colour-coded focal mechanisms: red = normal; blue = thrust/reverse; green = predominantly strike-slip, (b) well-constrained earthquake depths, colour coded as in (a). Filled circles are from analyses using MT5, and open circles are from wkbj. The dashed line, in this and in the following figures, shows the contour of zero dilatation from the strain-rate field calculated from the GPS velocities. Focal mechanisms from this study and from other sources are listed in the Supporting Information. The same scheme for marking different types of focal solutions is used in later figures.

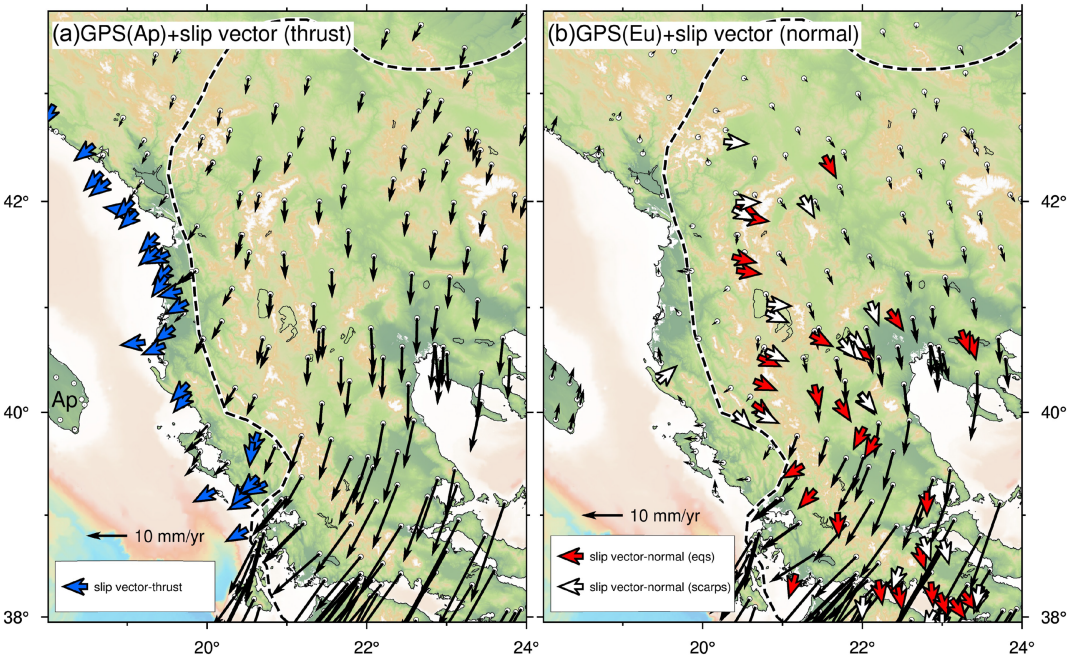

Figure 3. GPS velocity field (from D'Agostino *et al.* 2020) and Briole *et al.* (2021, see the text for details) and slip vectors from well-constrained moment tensor solutions. (a) GPS velocity field relative to Apulia and slip vectors of thrust-type earthquakes (in blue) along the Dinarides, Albanides and Hellenides. We systematically selected the slip vector direction lying on the low-angle east-dipping nodal plane that generally represents the overriding motion of the Balkans above the Adriatic/Ionian crust. (b) GPS velocity field relative to Eurasia and slip vectors of normal faulting earthquakes (in red) in the Balkans interior. White arrows show slip vectors measured from striations exposed on recently active fault scarps. The slip vectors represent the motion of the southern or eastern fault block with respect to the northern or western one. The isolated slip vector along the Albanian coast has been measured along the scarp of the Karaborun fault (Section 4.2).

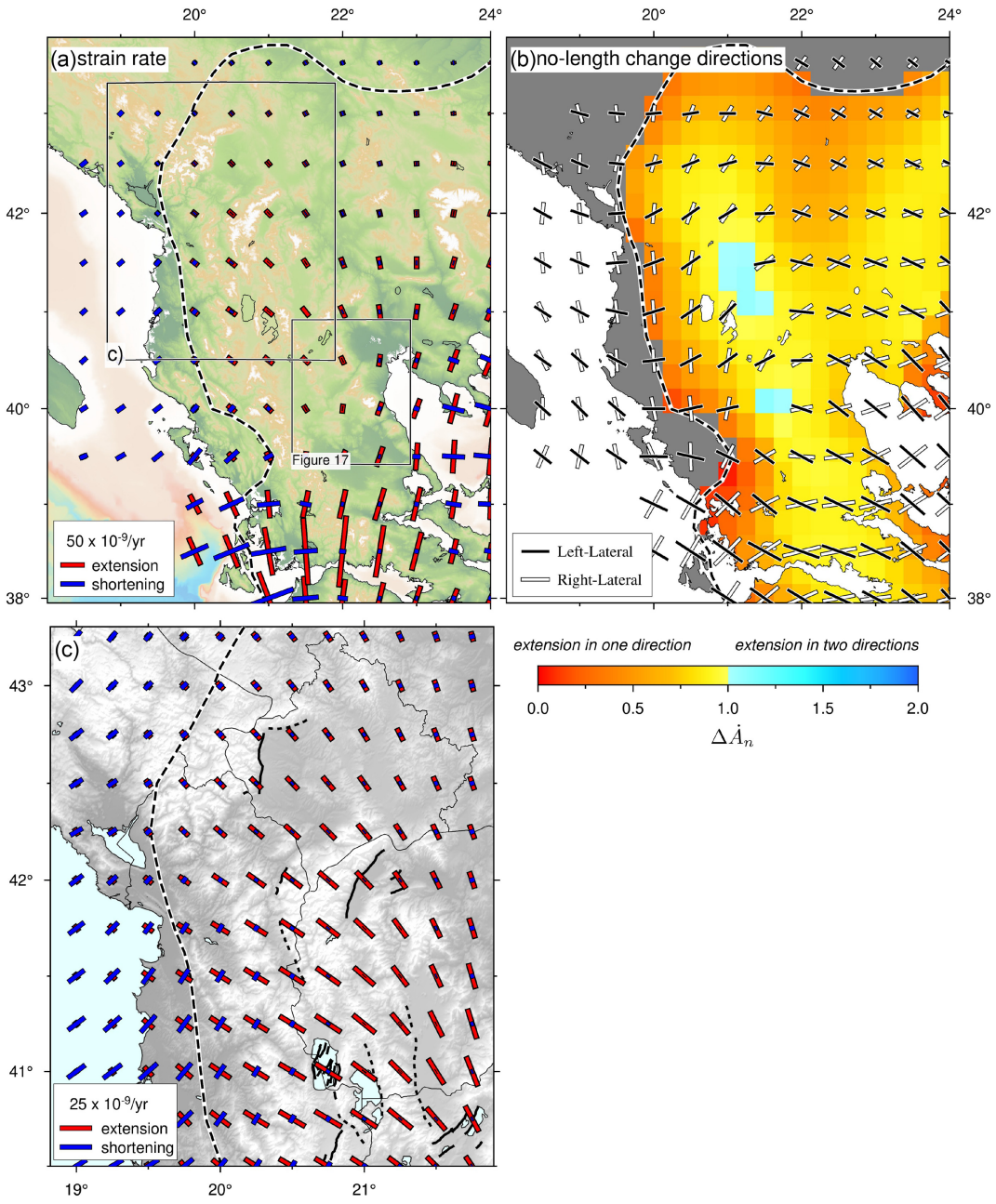

Figure 4. Strain rates obtained from the GPS velocity field (from D'Agostino *et al.* 2020). (a) Principal axes of the strain-rate field. (b) Directions of no-length-change. These directions show the two possible orientations of faults that can accommodate the strain rate field by uniform slip on faults of a single strike. Faults of the orientation marked by black bars would be expected to have some left-lateral slip, whereas faults marked by white bars would be expected to have some right-lateral slip. Colours within the extensional domain (south and east of the dashed line; see Fig. 2) are determined by the value of $\Delta\dot{A}_n$ (eq. 3). Grey shading shows where the largest principal axis is compressional. (c) Enlarged view of the strain-rate field in the NW Balkans.

Following Howell *et al.* (2017), we use the horizontal dilatation rate normalized to the largest (extensional) strain rate to map extending regions where the strain-rate field can be accommodated by a single set of parallel faults in two possible directions ($\Delta\dot{A}_n < 1$), or whether a minimum of two non-parallel sets is required ($\Delta\dot{A}_n > 1$), where:

$$\Delta\dot{A}_n = \frac{\dot{\epsilon}_1 + \dot{\epsilon}_2}{\dot{\epsilon}_1}, \tag{3}$$

and where $\dot{\epsilon}_1$ and $\dot{\epsilon}_2$ are the maximum and minimum eigenvalues of the principal axes of the horizontal strain-rate tensor respectively (extension positive). In Fig. 4(b), there are only two areas in which $\Delta\dot{A}_n \geq 1$, coloured in light blue, in the border region where Albania, Greece and North Macedonia meet, and in Thessaly, both of which show a distinct evolution of the faulting with time (discussed in Section 5). The value of $\Delta\dot{A}_n$ is close enough to 1.0 that, given the errors in the underlying GNSS velocity values and the effects of the above analysis, the values are not unambiguously ≥ 1.0. However, for the purposes of this paper, the key results is that the value of

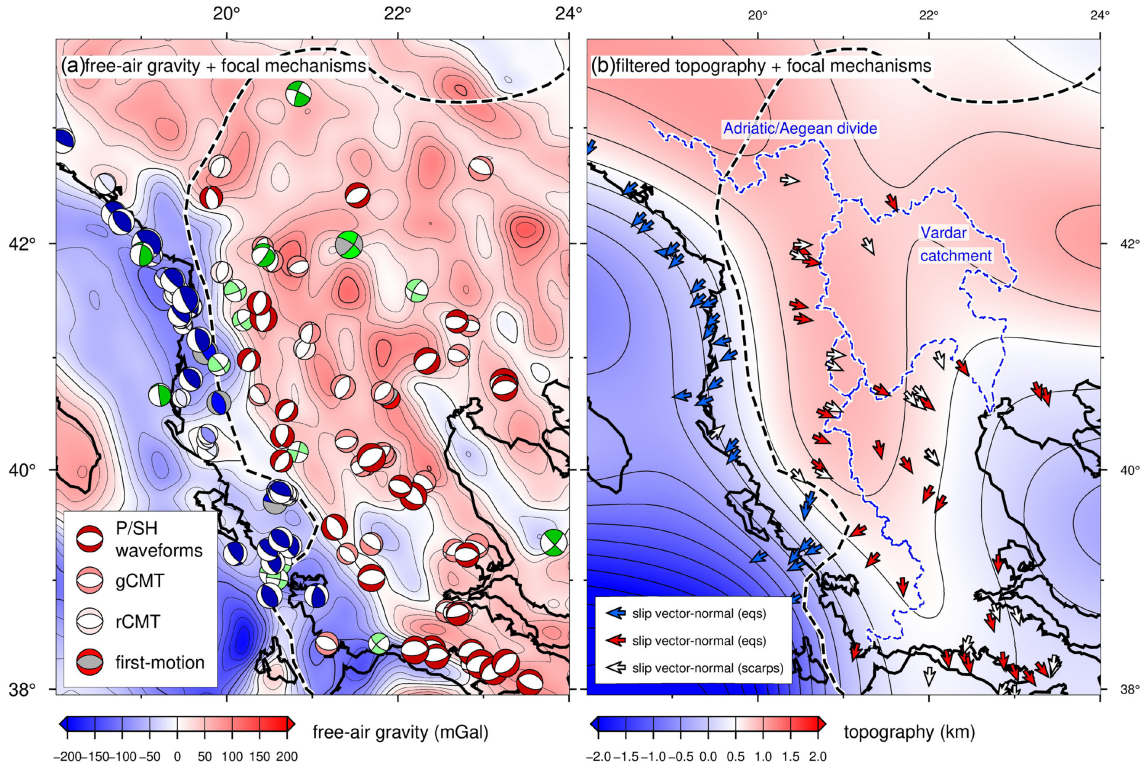

Figure 5. (a) Free-air gravity anomaly (Sandwell *et al.* 2014) and (b) smoothed topography obtained by the application of a Gaussian filter with full 6σ-width = 300 km. Earthquake focal mechanisms and slip vectors coloured as in Figs 2 and 3, respectively. The blue lines in (b) indicate major drainage divides.

$\Delta\dot{A}_n$ is greater in these regions than elsewhere in our study area, which is a robust result.

3 REGIONAL KINEMATICS FROM EARTHQUAKES AND GPS

Along the western coast of Albania and Greece, and seaward of an arc from SW Greece to the Hellenic Trench, we observe a relatively narrow (∼50 km wide) belt of active shortening with folding and earthquakes that have thrusting and reverse focal mechanisms (Fig. 2a and Fig.5). The earthquakes within this belt consistently display slip vectors aligned with the shortening direction of the geodetic strain-rate axes and with the motion of the Balkans relative to Apulia (Fig. 3a). The Kefalonia Transform Fault (KFT, Louvari *et al.* 1999; Shaw & Jackson 2010) terminates the belt of coastal shortening to the south and separates rapid (∼25–30 mm yr^{-1}) and mostly aseismic subduction of the deep oceanic Nubian lithosphere to the south from the slower (∼5 mm yr^{-1}) collision with the continental Apulian block to the north.

All the Balkan continental interior is characterized by crustal extension as far as north as 44°N, in Kosovo, Serbia and Northern Bulgaria as shown by the zero contour line of the dilatational strain rate estimated from the GPS velocity field (Figs 2–4; Kotzev *et al.* 2006; Burchfiel *et al.* 2006; Métois *et al.* 2015; D'Agostino *et al.* 2020). This wide region of crustal extension, included within the area of positive horizontal dilatation in Figs 2(a) and 4(a), is characterized by a progressive transition from NW-SE to N-S extension (Fig. 4c). A continuous belt of NW-SE extension, inland and parallel to the coastal contractional belt, runs along the highlands of Kosovo, the Albania-North Macedonia border (Ohrid and Prespa Lakes) and the mountain ranges in NW Greece (Epirus and Pindos), finally reaching central Greece. The separation between shortening along the Adriatic-Ionian coast and extension in the highlands is clearly marked by the contour of zero dilatation (Fig. 2a) that also separates extensional and thrusting focal mechanisms, showing the geodetic and seismological observations to be consistent. The transition from thrusting in the coastal lowlands to normal faulting in the highlands (Fig. 6) does not occur simply through the co-axial switch between the contractional and extensional axes along the maximum gradient of GPE, as would be expected in a 2-D force-balance controlled only by gravitational forces (Dalmayrac & Molnar 1981; Mercier *et al.* 1992; Copley *et al.* 2009; D'Agostino *et al.* 2014). Instead, D'Agostino *et al.* (2020) showed that the observed strain rate can be reproduced by the combination of a gravitationally driven E-W motion of the Albanian highlands towards the Adriatic and an N-S dextral shear imposed by the southward motion of the internal part of the Balkans relative to Eurasia. The combination of the two processes causes the transition between thrusting and normal faulting to occur through the reduction of the contractional NE-SW strain axis and concurrent increase of the NW-SE extensional axis (Figs 4c). Outside our region of study, east of 24° E, ∼N–S extension characterizes the internal part of the Balkans from the Greece-North Macedonia border to eastern Bulgaria, in a wide region called the 'South Balkan Extensional System' by Burchfiel *et al.* (2008, further references therein).

In the extensional part of our study region, the velocity field is generally characterized by only one extensional principal axis of the horizontal strain-rate tensor ($\Delta\dot{A}_n < 1$), which can be achieved by a single set of parallel faults (Fig. 4b). Only in North Macedonia and northern Greece, where the extension direction changes from NW–SE to N–S, $\Delta\dot{A}_n$ is slightly greater than 1 in two limited areas. In this region we observe focal mechanisms and slip vectors with rapidly changing patterns, sometimes with orthogonal directions of

extension within spatial scales less than a few tens of kilometres (Figs 2a and 3b). An ∼E–W trending set of active faults frequently cuts across pre-existing N–S or NW–SE oriented fault systems, whose relative geomorphological characteristics also attest to less recent activity on the N–S or NW–SE faults (Mercier *et al.* 1989; Pavlides & Mountrakis 1987; Caputo & Pavlides 1993; Caputo *et al.* 1994; Burchfiel *et al.* 2008; Goldsworthy *et al.* 2002). These earlier Quaternary, but currently inactive, N–S or NW–SE structures frequently control the regional physiographic features (mountain ranges and coastline) and the geometry of the larger sedimentary basins (e.g. Karditsa and Larissa Basins, Caputo *et al.* 1994).

The GPS velocity field shows a 150–200 km wide band of NE-SW right-lateral shear, roughly centred on the North Aegean trough (NAT, Fig. 1), reaching from the NE Aegean, through central Greece, to the NW termination of the Hellenic subduction zone (McClusky *et al.* 2000). In the NE and SWm this motion is achieved by parallel NE–SW strike-slip faults (Taymaz *et al.* 1991; Hatzfeld 1999) parallel to the NAT and Kephalonia Transform Zone, respectively. In central Greece the discrepancy between the generally N–S slip vectors on the E–W normal faults and the overall NE–SW motion suggests that those faults rotate clockwise as they move (McKenzie & Jackson 1983, 1986), a configuration achieved by the strike-slip faults terminating in grabens that die out towards the centre of Greece (Goldsworthy *et al.* 2002), with a strong focusing of N–S extension (varying ∼ 5–15 mm yr^{-1} from E to W) across the Gulf of Corinth (Armijo *et al.* 1996; Clarke *et al.* 1997). Overall, central Greece acts as a relay zone connecting the strike-slip faults in northern Aegean with those on the Ionian side to accommodate the rapid motion of the northern Aegean and Anatolia towards the Hellenic Trench. The southern Aegean Sea (or Sea of Crete: roughly 36–38° N, 24–27° E), where extension has reduced the crustal thickness to ∼20–25 km (McKenzie 1978), is now characterized by extremely low geodetic strain rates (McClusky *et al.* 2000; Reilinger *et al.* 2010). Active extension and crustal thinning are now active on both the western and eastern margins of the Aegean Sea, where crustal thickness still exceeds ∼25 km (Sodoudi *et al.* 2006; Zhu *et al.* 2006).

4 THRUSTING IN THE ALBANIDES AND HELLENIDES

Thrust-faulting earthquakes indicate active crustal shortening all along the western margin of the Adriatic Sea from the Dinaric coast to the island of Kephalonia (Fig. 2a; Baker *et al.* 1997; Louvari *et al.* 2001; Benetatos & Kiratzi 2006; Copley *et al.* 2009). The GPS-derived strain-rate field (Fig. 2a) shows that the line separating horizontal positive (extension) dilatation in the highlands from negative (shortening) dilatation in the coastal lowlands also runs along the Albanides and Hellenides. The line is very close to the coast near NW Albania, moving inland along the Albanides–Hellenides and finally aligning with the Kephalonia Transform Zone, consistent with the strike-slip character of this structure (Shaw & Jackson 2010). The coastal shortening belt is at its widest (∼ 40 km) close to the Greece-Albania border.

It has been suggested (Roure *et al.* 2004; Argnani 2013; Bega & Soto 2017) that the structural style of the external part of the Albanides and Hellenides fold-and-thrust belts, and the evolution of the related foredeep basins, are strongly controlled by the nature of the Mesozoic units (the Apulian platform and its adjacent deep-water basins). In this section, we describe the active shortening structures along the collisional sector of the Hellenic arc, where the lithosphere of the Apulian and Ionian zones is overthrust along the Dinarides, Albanides and Hellenides convergent belts. Our focus is on the role of (i) the Mesozoic palaeogeography in the Apulian and Ionian domains and (ii) the transverse structures (Scutari-Pec, Vlora-Elbasan; see Figs 1 and 7) in controlling the continuity and segmentation of on the main active shortening features of the collision front. We also consider (iii) the dynamic significance of extensional faults observed within the contractional belt on the Karaborun peninsula (KP in Fig. 1).

4.1 Crustal shortening along the Dinarides, Albanides and Hellenides

The largest instrumentally-recorded earthquake in the southern part of the Dinarides is the 1979 Montenegro event (M_s 6.9, Fig. 7a), whose source parameters and location indicate a NE-dipping low-angle (∼15°) fault plane projecting to the surface seaward of the Adriatic coast (Baker *et al.* 1997; Benetatos & Kiratzi 2006). Geological studies and seismic reflection lines (Bega & Schleder 2017; Schmitz *et al.* 2020) point to the offshore part of the inferred Dalmatian Thrust as the fault responsible for the earthquake. Little internal deformation is seen in GPS velocities landward of the Adriatic coast in Montenegro (Fig. 7b), suggesting that elastic strain accumulation is mostly confined offshore, consistent with the 1979 earthquake location.

SE of Skhoder, the Dalmatian Thrust continues onshore where the shallow-water Mesozoic carbonates of the Kruja unit (Velaj 2012) override the Neogene sedimentary infilling of the Peri-Adriatic Depression (PAD, Roure *et al.* 2004) with no evidence of recent activity. The PAD, clearly expressed by a distinct negative free-air gravity anomaly (Fig. 7a), is filled with 7–10 km of Oligocene-Quaternary sediments (Roure *et al.* 2004) interpreted to be the flexurally controlled foredeep in front the advancing Albanides nappes (Roure *et al.* 2004; Argnani 2013). Correlation with the palaeogeographic boundaries of the Mesozoic Southern Adriatic Basin (Argnani 2013; Arizaga *et al.* 2017) suggests that inheritance of Mesozoic lithospheric structures in the Southern Adriatic may have also controlled the later Tertiary evolution and the geometry of the flexural Oligocene-Quaternary basin, as the basin and onshore PAD are confined between the edges of the Mesozoic Dalmatian and Apulian carbonate platforms (Fig. 7b). Geological mapping (Xhomo *et al.* 2002) and seismic reflection lines (Argnani 2013; Bega 2015) show intense folding (anticlinal axes marked in Fig. 7c) and backthrusting affecting the sedimentary infilling of the PAD above a detachment horizon localized at the base of the clastic sequence (Oligocene shales of Roure *et al.* 2004). The transition from the Dinarides to the Albanides is traditionally placed across the Scutari-Pec (Skhoder-Peja; SP in Fig. 1) transverse line, which separates unrotated Dinarides units from the Albanides units, which have rotated clockwise by up to 50° since the Lower Miocene (Kissel *et al.* 1995; Speranza *et al.* 1995). The Dinarides–Albanides transition is also expressed by a marked change in orientation of the coastline and by the right-stepping en-echelon arrangement of the anticline axes deforming the Neogene-Quaternary sedimentary infilling of the PAD. An example of a well-constrained earthquake in the Albanides is the 2019 Durres (M_w 6.4) event (Fig. 7a), whose body-wave moment-tensor solution, INSAR and GPS signals indicate an E-dipping low-angle (13°) thrust fault at 23 km depth as the causative fault plane (Fig. S9, Supporting Information; Papadopoulos *et al.* 2020; Vittori *et al.* 2020). The presence of Neogene anticlines associated with W-dipping high-angle backthrusts

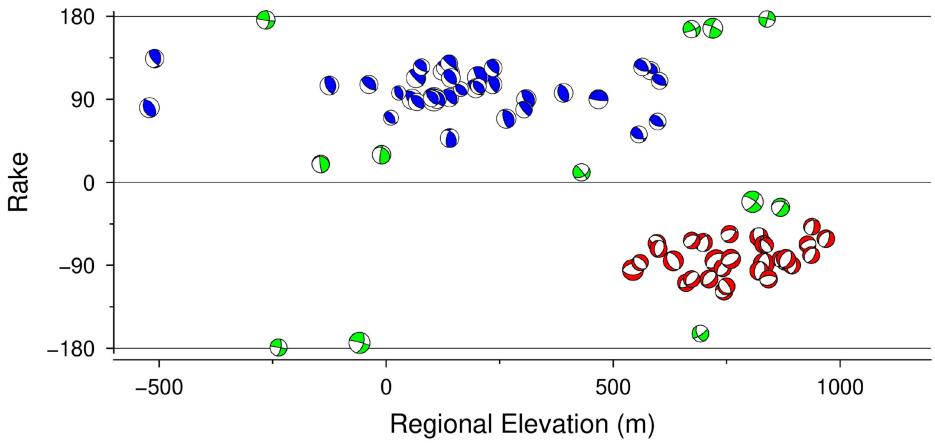

Figure 6. Elevation distribution of focal mechanisms according to regionally filtered topography (Fig. 5b). Focal mechanisms have been selected within the thin-dashed box in Fig. 2(a).

suggests that the shallow Oligocene-Quaternary sequence is decoupled from its deeper Mesozoic part at the level of the Oligocene shales (Roure *et al.* 2004). The influence of the Mesozoic facies distribution and the heterogeneous thickness of Tertiary sediments is clearly expressed in the depths of well-constrained thrust-faulting earthquakes along the Adriatic and Ionian margins. As shown in Fig. 7(d), thrust-faulting earthquakes within the PAD are confined to basement in the depth range 15–30 km, while the thick sediments appear to deform largely aseismically: a situation known from elsewhere like the Caspian Sea and Bengal Fan (Jackson *et al.* 2002; Kumar *et al.* 2015). In this case, the earthquakes are probably confined to the crystalline basement beneath the Mesozoic carbonates and their overlying Oligocene-Neogene clastic sequence.

SE of the PAD, crossing the Mesozoic palaeogeographic boundary between the Southern Adriatic Basin and the Apulian Platform (Fig. 7b), the coast changes orientation back to NW–SE. A shortening gradient in SW-directed GPS velocities in Fig. 7(b) indicates elastic strain accumulation on NW–SE striking thrust faults that is likely to be released seismically (Valkaniotis *et al.* 2020), perhaps rupturing the seafloor close to the Ionian islands with significant tsunamigenic implications. A well-constrained thrust earthquake at 24 km depth (39.8° N 20.6° E; Figs 2 and 7b) indicates that the Hellenides fold-and-thrust belt is seismically coupled at depth for tens of kilometress inland from the Ionian coast. At shallower levels in NW Greece and SW Albania the long, linear concentric folds in the Mesozoic platform carbonates, which dominate the surface morphology, are likely to be decoupled from deeper structures by Triassic salt (IGRS-IFP 1966). Our observations do not support the active role of a dextral transfer zone between Vlora and Elbasan (Fig. 7b; Handy *et al.* 2019). The lack of well-constrained strike-slip fault-plane solutions and the smoothness of the boundary separating geodetic extension in the Albanian highlands from crustal shortening in the coastal lowlands, do not appear to require any first-order discontinuity along the Albanides thrust front corresponding to a line joining Vlora and Elbasan (Fig. 7b).

4.2 Time-dependent crustal shortening in the Karaborun peninsula?

On the eastern side of the mountain ridge defining the KP (in Figs 1 and 8a), we observed a NW–SE-striking fault scarp in limestone, extending for ∼15 km along the base of the mountain front (Fig. 8b). Streams dissecting the range front leave narrow wine-glass canyons between truncated spurs with triangular facets that suggest the extensional nature of the fault (Fig. 8c). The scarp is defined by both a well-preserved bedrock scarp, similar to the postglacial scarps observed in Greece and in the Apennines (Goldsworthy & Jackson 2000; Caputo *et al.* 2006; Tucker *et al.* 2011), and by a 1–5 m high scarp in an alluvial fan composed of unconsolidated debris ∼2 km WNW of the village of Dukat i Ri. Clear fault-plane exposures can be seen at various points along the fault, containing many of the features typical of normal fault surfaces in the Aegean, including a cut and polished cemented-breccia surface, striations and corrugations (Hancock & Barka 1987). The exposures of the fault plane show the contact between carbonate bedrock and sheared colluvial deposits lying directly on the fault surface and dip-slip extensional striations with azimuth N48 (Fig. 8d). To the north, the bedrock fault scarp can be followed crossing the saddle of the peninsula at a small bay on its western side (Figs 8b and e).

These observations suggest recent activity (Late Quaternary-Holocene) of the fault. On the other hand, the extensional character of the observed fault scarp contrasts with seismological and geodetic evidence for a dominantly contractional regime along the Albanian coast. The normal fault on the KP indicates that, at least at shallow levels, there is localized extensional strain at this place. Yet, the temporal relationship of the extensional strain with the geodetically observed contraction along the Albanian coast is unclear. Three general explanations for the formation of the Karaborun fault can be envisioned:

(i) It is simply a superficial normal fault on top of a thrust or fold, which would not be surprising in a massive carbonate sequence deforming by concentric folding in response to a large thrust earthquake. This process is well known and has been observed, for example, in the 1980 El Asnam, Algeria (Yielding *et al.* 1981) or the 1994 Sefidabeh, Iran (Berberian *et al.* 2000) events. However, in contrast to the relatively minor extensional scarps observed in those earthquakes, the scarp observed along the KaP is longer, more continuous, and must have moved in repeated events to generate the topography in Fig. 8(c).

(ii) The KP is at the transition from Mesozoic basin to carbonate-platform sequences at the frontal mountain range (Argnani 2013), and is well expressed on both the topography and gravity maps (Figs 7a and b). The observed normal faulting could correspond in to a local collapse structure on top of high ground, aided by this lithological boundary.

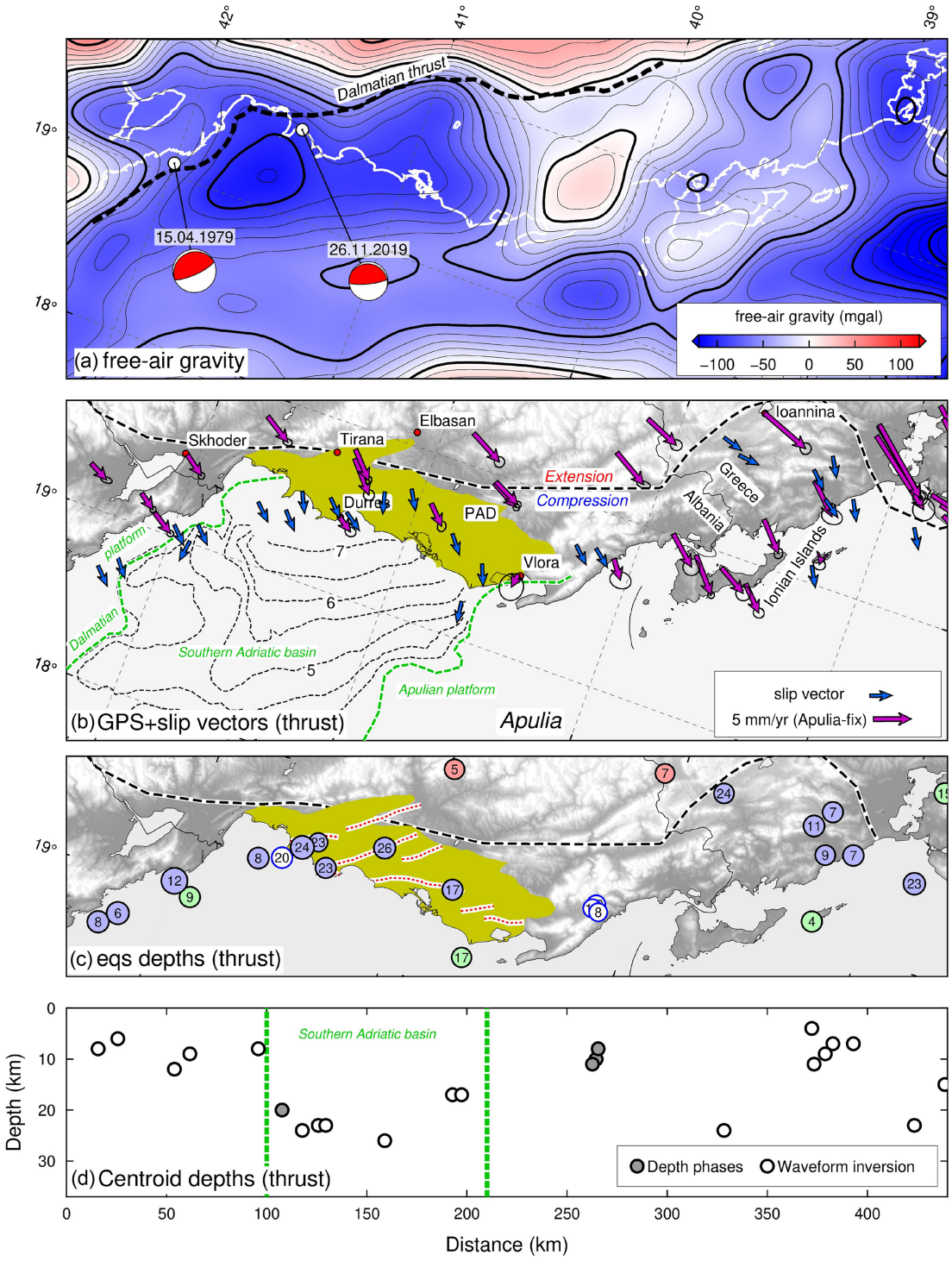

Figure 7. (a) Free-air gravity anomalies (Sandwell *et al.* 2014) of the collisional boundary of the Dinarides–Albanides–Hellenides zone and focal mechanisms of the largest well-constrained earthquakes. The black dashed line shows the trace of the Dalmatian Thrust, and the white line is the coast. (b) GPS velocity field (red, relative to Apulia) and slip vectors of well-constrained earthquakes (blue). Dashed lines offshore show Mesozoic palaeogeographic boundaries between carbonate platforms and basinal units (in green) and TWT contour lines (in seconds) of the top of Mesozoic carbonates (both from Arizaga *et al.* 2017). The PAD is emphasized in yellow. (c) Distribution of earthquake depths from waveform inversion or depth-phase analysis. Colour scheme is the same as Fig. 2(b). The trace of anticlinal axes within the PAD are shown with red dashed lines. (d) Same as (c) with depth along the y-axis. The green lines show the extent of the Mesozoic Southern Adriatic Basin.

(iii) It is time-dependent faulting, and is active following co-seismic stress relaxation following a large earthquake on an underlying thrust, as observed, for example, in Chile (Farías *et al.* 2011) and in Japan (Asano *et al.* 2011; McKenzie & Jackson 2012). Such time-dependent deformation of the overriding plate requires the thrust fault to be locked, to release all the accumulated elastic shortening strain, and to move in earthquakes, rather than sliding continuously.

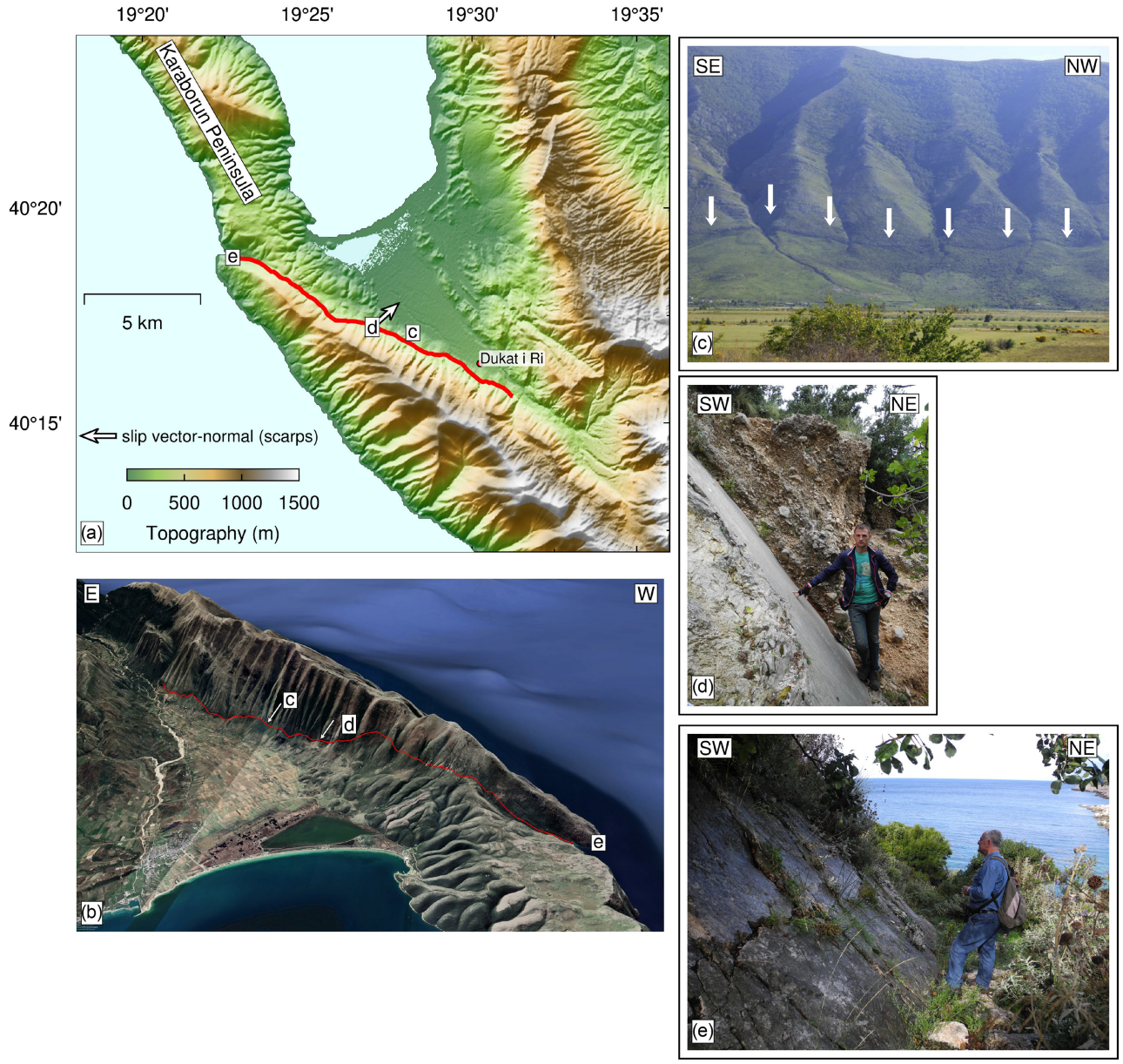

Figure 8. Active normal faulting along the KP. (a) AW3D30 ALOS topography and main physiographic units and relevant locations shown in pictures (c)–(e). The red line shows the trace of the active normal fault forming a continuous scarp along the base of the NE side the mountain range forming the southern part of the KP. The white arrow shows the direction of the slip vector measured on the exposure of the fault surface shown in (d), at 40.2873°N, 19.4497°E. (b) Google Earth image of the KP. The active fault crosses the mountain ridge to where it is exposed in the small bay (e, 40.3145°N, 19.3792°E).

Only the last two options are likely to cause the normal fault overlying the thrust to move in repeated separate normal-faulting earthquakes. In the southern part of the Dinarides, within the epicentral area of the 1979 Montenegro M_s 6.9 earthquake, Biermanns *et al.* (2022) describe SW-dipping normal faults with evidence of Quaternary activity in the hangingwall of the fault likely to have been responsible for the 1979 event. Late-Quaternary E–W normal faults that presumably only move after big E–W thrust earthquakes (Shaw *et al.* 2008) have been also observed in Crete (Caputo *et al.* 2010). These various observations may therefore indicate a general condition of the collision/subduction interface along the Hellenic Arc wherein compressional deviatoric stresses sustained along the coastal belt can, after major thrust events, switch temporarily to horizontal extension. This inferred stress state requires the present tectonic stress transmitted across the collision/subduction thrust faults to be low, comparable to the stress drops observed in earthquakes, and has implications for the support of the topography of the Aegean that will be discussed below.

5 ACTIVE CRUSTAL EXTENSION IN THE BALKAN HIGHLANDS

In this section, we report field observations of active normal faulting and associated tectonic features in the west Balkan interior of Albania, Kosovo and Republic of North Macedonia that add to the few published studies described below. Our main concern is to present information on the relative state of activity of the faults within the system, the direction of extension inferred from field observations

and its comparison with seismological and geodetic data, as well as evidence for changing spatial and temporal patterns of that activity. In Greece there are many published studies of the active faults we can refer to (e.g. Goldsworthy *et al.* 2002; Caputo & Pavlides 2013; Ganas 2020), but the internal Balkan region of Albania-Kosovo-North Macedonia has attracted less attention and has been scarcely studied. In the following, we describe fault systems which have not previously been reported and are relatively unknown, or present new observations that reinforce inferences presented in previous studies. Our criteria to evaluate relative fault activity are based on the observations of range-front and fault-scarp morphology, associated drainage and kinematic indicators on exposed fault surfaces suggesting recent fault slip (Wallace 1987; Goldsworthy & Jackson 2001).

5.1 The Dukagjini–Kosovo basin

The Dukagjini basin (Fig. 9a) is one of the main physiographic features of the Balkan interior and is bounded to the north and to the east by prominent range-bounding normal faults. The basin is filled with a ∼1500 m thick Neogene-Quaternary continental sedimentary sequence intercalated with lignite levels (Elezaj 2009, 2010), whose architecture is controlled by the activity of the two range-bounding normal faults, recording the sustained and prolonged activity of the basin during the Neogene-Quaternary period. The sediments within the basin are slightly tilted to the west and thicken towards the boundary faults at the western margin of the basin (Elezaj 2009). The main fault system controlling deposition in the Kosovo basin is oriented N–S (the Peja/Pec segment), changing in the northern part to a ENE–WSW strike (Istog segment).

The basin is located at the northern edge of the extending continental interior of the southwestern Balkans (Figs 2 and 3) and represents the northernmost fault system with a morphologically clear expression of active extension. No historical source provides evidence of large earthquakes in the past that can be associated with particular faults in this region (Ambraseys 2009). We observed signs of recent activity along the N–S part of the fault south of Peja, where streams dissecting the range front leave narrow wine-glass canyons between truncated spurs with triangular facets (Fig. 9b). Direct exposures of the fault surfaces and striations are rare but were found at the base of the mountain front where the apex of a scree cone originates from a narrow wine-glass canyon (Fig. 9c). The northern, ENE–WSW part of the fault system bounding the Kosovo basin shows no significant evidence of recent activity. By contrast, in that area exposure in a quarry along the fault (Fig. 9d), shows that colluvial debris covered and reworked the fault surface, suggesting the absence of recent slip along that part of the fault. These observations suggest the N–S part of the basin-bounding fault, accommodating an approximate E–W extension, is more active than the ENE–WSW segment. This inference is also consistent with the extension directions inferred from two fault-plane solutions located a few km to the west of the Kosovo basin (Fig. 2a) and with the directions of the geodetic strain-rate axes (Fig. 4c).

5.2 The Kukes region and the Black Drin river valley

Geomorphological observations by Copley *et al.* (2009) suggested that the present course of the Black Drin river is controlled by active normal faulting along the ∼N–S-striking range-bounding fault which is discontinuously exposed along the eastern side of the valley (Fig. 10). Dry wind gaps (blue filled circles in Fig. 10) along the mountain range to the west of the valley suggest that a former west-directed drainage system was disrupted by the activity of this normal fault system. Direct evidence of active faulting has been observed near Bicaj village along the Black Drin river (Fig. 11a). Exposed fault scarps at the base of the mountain front reveal striations with azimuths between N90 and N116 on fault surfaces recently quarried for road works (Fig. 11b) or naturally exposed (Fig. 11c). A cumulative fault scarp ∼2–3 m high (Fig. 11d) observed at the contact between the carbonate bedrock and the lower part of the slope in cemented colluvial debris suggests repeated episodes of postglacial co-seismic exhumation of the fault surface. Near Debar a 10 km-long, ∼50 cm scarp was reported by Sulstarova & Koçiaj (1980) for a normal faulting event of M_w 6.2 in 1967 [the southernmost earthquake mechanism in Fig. 10, well constrained by body-wave modelling (Baker *et al.* 1997)]. This region is remote and difficult to access, but even allowing for poor preservation of fault morphology in steep, mud-rich flysch that is very prone to landslides, we could not find the rupture or signs of well-developed, cumulative fault-controlled structures. The similarity with the other focal mechanisms within an elongated N–S region of higher strain rates (Figs 2 and 4a) suggests the continuity of a belt of NW–SE extension between the Dukagjini-Kosovo basin and the Korca basin (described below) in the south, following the Albanian border with Kosovo, North Macedonia and Greece.

5.3 The Tetovo graben and Rashche fault

The Tetovo graben (Fig. 10) is one of the clearest expressions in the western Balkans of a range-bounding mountain front formed by normal faulting. The basin is elongated in an NNE–SSW direction for ∼50 km in the northeastern part of Northern Macedonia near the Kosovo border. The morphology of the range-bounding fault is typical of active normal faults observed in crystalline/schist lithology in Greece (Goldsworthy & Jackson 2000), with the fault forming a sharp linear edge that bounds the plain and is clearly the dominant feature in the morphology. Streams flowing off the fault scarp incise into the footwall, giving the front a dissected appearance leaving narrow wine-glass canyons between truncated spurs with triangular facets, as also seen in the Dukagjini–Kosovo basin (Fig. 9b). Alluvial fans along the densely inhabited base of the mountain front are frequently truncated and suspended above the plain, suggesting sustained activity of the range-bounding fault. A NW-SE extension direction is consistent with the geometry of the fault-controlled basin, but the only available earthquake fault-plane solution is 30 km along strike to the NE.

The Vardar river exits the Tetovo graben to the north, passing through the Skopje basin, struck in 1963 by an M_s 6.3 earthquake for which only a first-motion strike-slip fault-plane solution is available (Fig. 10). East of the Tetovo graben we observed limestone fault scarps near the village of Rashche with evidence of Late Quaternary activity and fresh striations on the mirror-like fault scarps (Fig. 12). The slip vector measured on the fault plane indicates an N150 direction, more southerly than the E–W extension directions observed along the eastern Albanian border, and similar to the N–S extension direction found in the central and eastern parts of North Macedonia. An M_w 4.9 gCMT solution in the southern part of the Tetovo graben (Fig. 10) also displays a more southerly extension direction similar to the solutions observed in the eastern part of Northern Macedonia. In the western part of Northern Macedonia along the Albanian border we thus observe a progressive clockwise rotation of the extension directions from WNW–ESE in Albania to NNW–SSE in central-eastern North Macedonia (Fig. 3b).

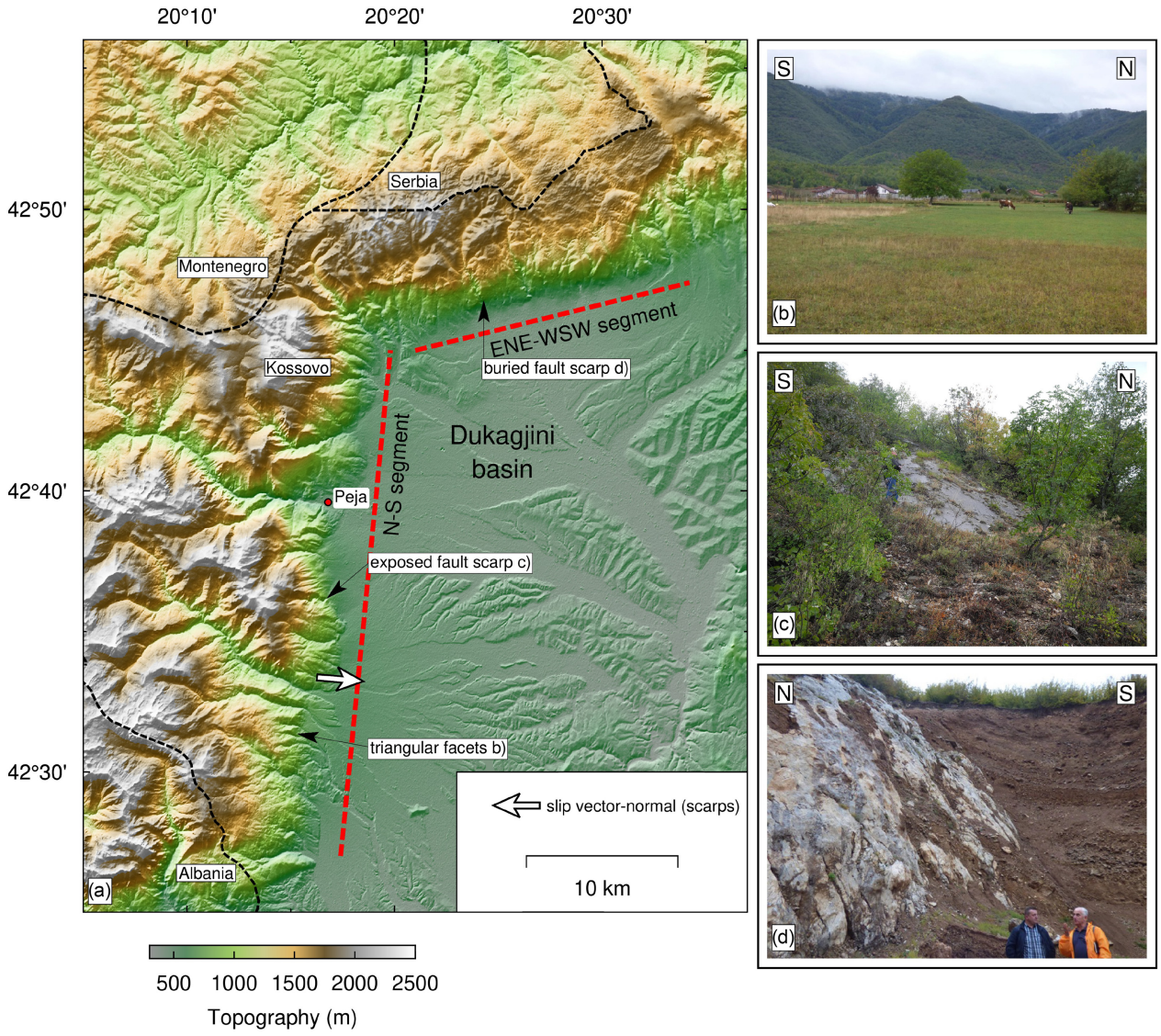

Figure 9. Active normal faulting and geomorphology of the Dukagjini (Kosovo) basin. (a) AW3D30 ALOS topography and main physiographic features and evidence of active normal faulting. The large white arrow indicates the direction of the slip vector measured on the striated fault surface. (b) Triangular facets along the N–S trending range-bounding fault (observed from 42.5143°N, 20.2910°E). (c) Striated fault surface exposed at the base of the N–S trending range-bounding fault (42.6032°N, 20.2797°E). (d) Colluvial deposits covering the eroded, reworked and excavated scarp of the E–W trending range-bounding fault (42.7785°N, 20.4049°E).

5.4 The Korca–Ohrid fault system

The clearest field evidence of normal faulting in the Albanian highlands is observed in the region of Lake Ohrid and Korca (Figs 13 and 14). Internal drainage and continuous stratigraphy in Lake Ohrid over the last 2 Myr (Lindhorst *et al.* 2015) indicate persistent local subsidence and normal faulting. The basin occupied by Lake Ohrid is bounded to the east by the high Galicia mountain range whose western slope is formed by a system of stepped W-dipping faults with evidence of recent activity (Hoffmann *et al.* 2010; Reicherter *et al.* 2011; Hoffmann 2014) with striations of azimuth N100–120, exposed on fresh bedrock fault scarps. Seismic-reflection profiles and bathymetry surveys in Lake Ohrid, have also found evidence of normal faulting within the lake (Lindhorst *et al.* 2015), with recent sediments and the lake floor displaced by both east- and west-dipping extensional faults, consistent with a symmetrical graben architecture. The Korca basin is bounded by an east-tilted fault block (Morava mountain) with ophiolitic rocks covered unconformably by Palaeogene-Neogene deposits of the Mesohellenic Trough (Xhomo *et al.* 2002). Evidence of recent activity, including triangular facets, wine-glass suspended valleys, and fault scarps at the base of the mountain range, are concentrated near and south of Korca and have been described by Dufaure *et al.* (1999). WNW–ESE slip vectors measured along the Korca fault, and along the fault bounding Lake Ohrid, are similar to that of a well-constrained focal mechanism for an earthquake of M_w 5.1 in 2009, a few km SW of Korca (Fig. 14).

The Lake Ohrid and Korca basins display geomorphology and drainage systems that are typical of basins formed along the crest of a mountain belt that is now extending by normal faulting (e.g. D'Agostino *et al.* 2001; Geurts *et al.* 2018; Wimpenny *et al.* 2020), and also suggest an evolution of the faulting with time. In such places the position of the regional drainage divide generally corresponds with the highest smoothed elevations and with the more active normal faults which, by repeated fault motion may create

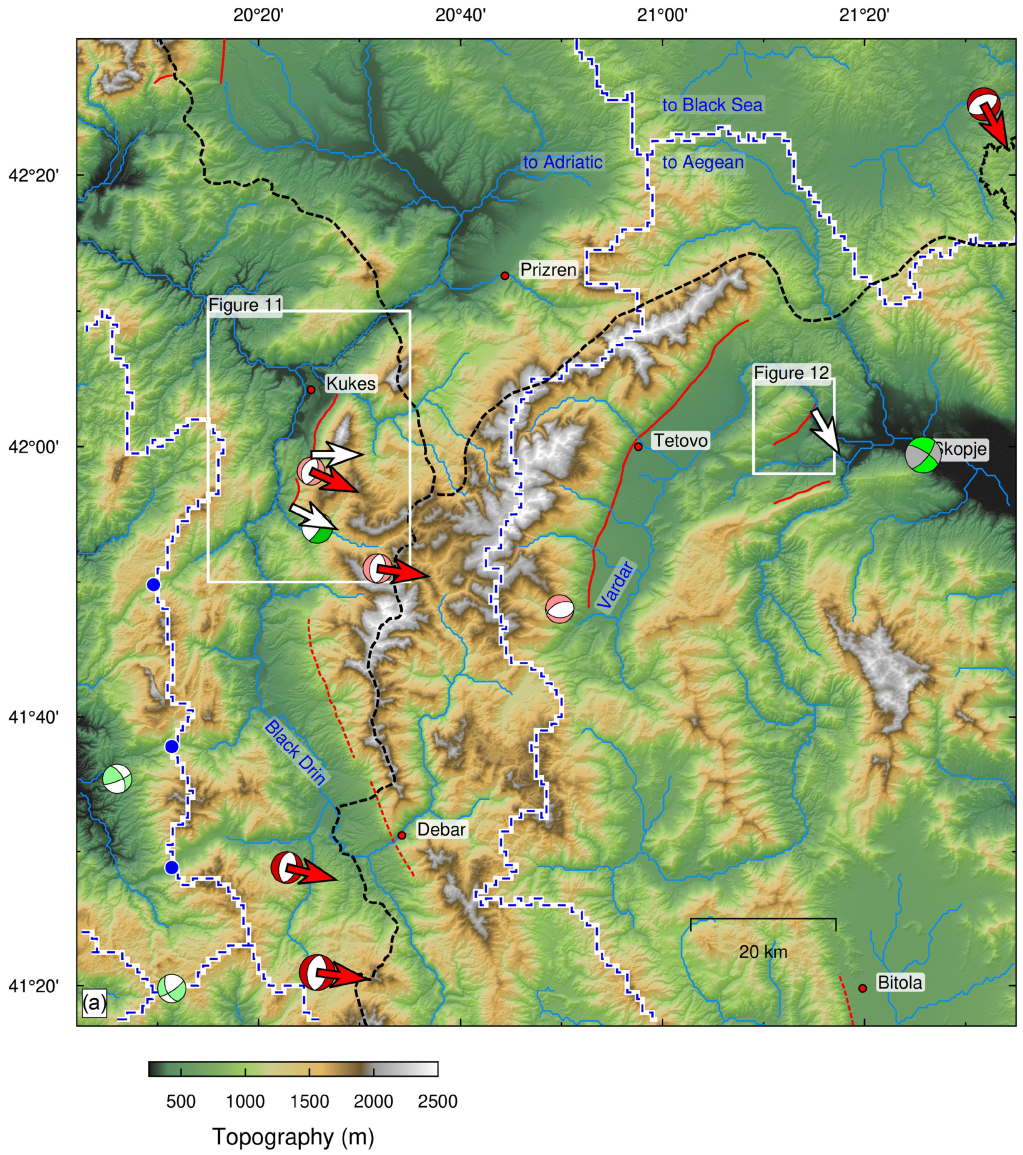

Figure 10. Topography and morphology of the Albanian and North Macedonia highlands. Continuous and dashed red lines mark the active and relatively inactive fault systems, respectively. Blue dashed lines show major drainage divides; black dashed lines are international borders. Focal mechanisms follow the same scheme shown in Fig. 2. Blue circles along the westernmost drainage divide indicate wind gaps along the mountain ridge to the west of the Black Drin river valley, suggesting the disruption of a former west-directed drainage system.

internally drained basins that can, for a while, resist capture by the headward incision of rivers from their surrounding lower elevations (D'Agostino *et al.* 2001). Eventually, however, the fate of such internal basins straddling the main divide is ultimately to be captured, incised and emptied of their sedimentary fills. The map of filtered topography (Fig. 5b) shows that the trace of the drainage divide between the Adriatic and Aegean roughly follows the highest elevations and the zone of fastest extension (dilatation) on the edge of the highest western Balkans (Fig. 4b). The two Prespa Lakes occupy an internal basin, trapped by subsidence on the Baba Fault and footwall uplift on the Ohrid and Mali Thate faults (Fig. 14a), straddling the main west Balkan drainage divide. The Korca basin may have once occupied a similar position, isolated in the hangingwall of the Korca Fault and including a natural swamp area near Maliq which was a shallow lake until it was finally drained after 1948 (Dufaure *et al.* 1999). The basin has now been captured by headward incision by the Devolit river, which drains to the Adriatic, leading to a contrast between the relatively incised Maliq region and the relatively undisturbed upper Korca basin. Unlike the NNE–SSW Ohrid-Korca faults, with their abundant freshly exposed fault planes, the NW–SE Mali Thate fault shows no sign of recent activity, and is more subdued in the landscape. We suspect that activity has recently switched from the NW–SE Mali Thate fault to the NNE–SSW Ohrid-Korca system, probably in response to the (perhaps changed) regional velocity and strain-rate fields (Fig. 4): the NW–SE current extension seen in the GPS strain rates cannot easily be accommodated by a fault of that strike, whereas the NNE–SSW faults can do so. We discuss more evidence of changing fault systems below.

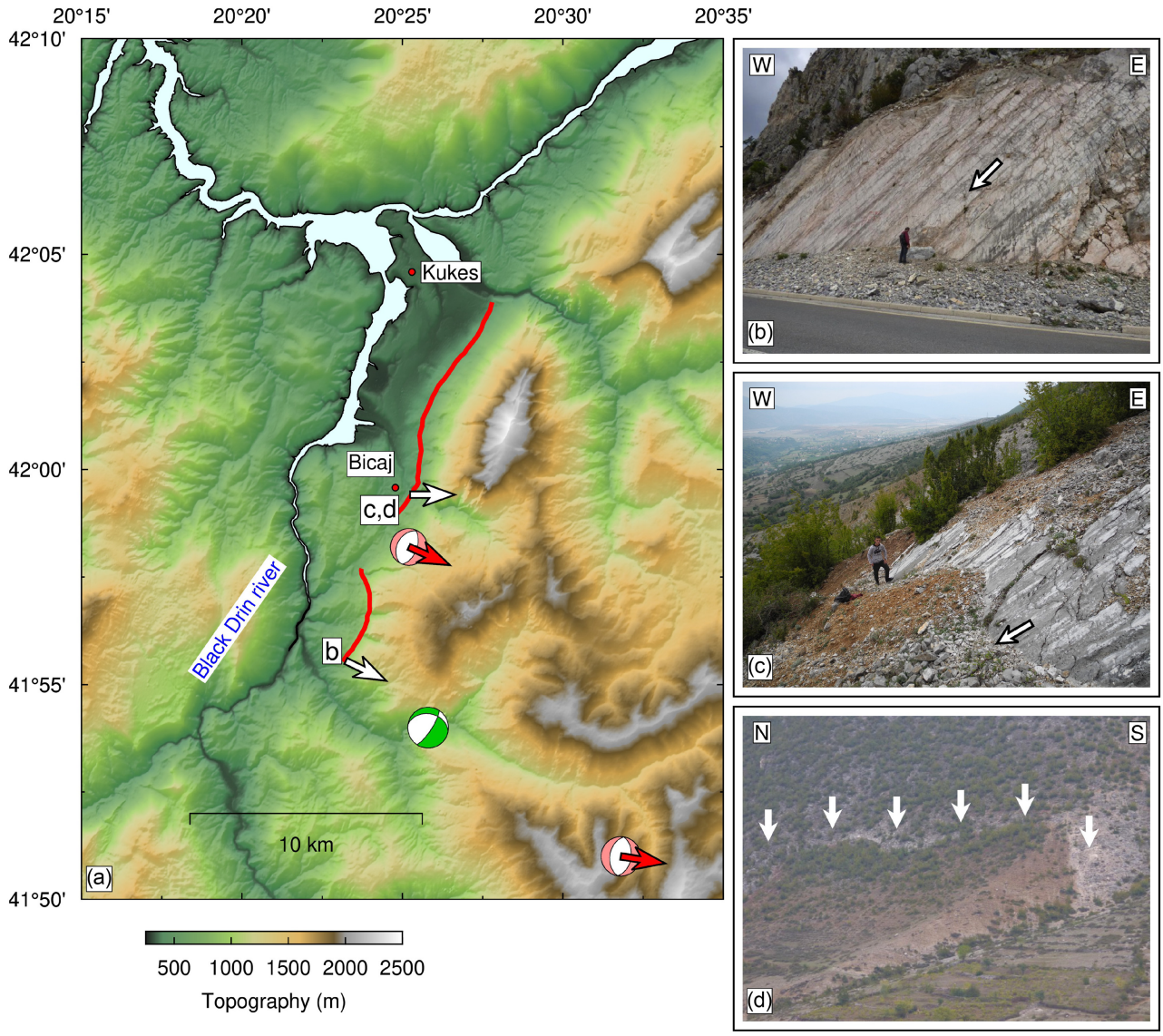

Figure 11. Active normal faulting in the Kukes region. (a) AW3D30 ALOS DEM and main physiographic features and evidence of active normal faulting. The white and red arrows indicate the directions of the slip vector measured on the striated fault surface and from body-wave modelling respectively. Colours of the compressional quadrants follow the same categories shown in Fig. 2. Photos in (b, 41.9263°N, 20.3866°E) and (c, 41.9944°N, 20.4253°E) show exposed bedrock fault scarps where the directions of the slip vectors have been measured. White arrows indicate the direction of the slip vector on the fault surface. (c) Bedrock fault scarps indicated by vertical white arrows near the village of Bicaj (41.9954°N, 20.4252°E).

5.5 The Florina–Ptolemais–Servia graben

The NNW–SSE Florina–Ptolemais–Servia (FPS) graben system (Fig. 13) is a part of a ∼150 km long extensional structure crossing the border between Republic of North Macedonia and Greece (Metaxas *et al.* 2007). The stratigraphy of the basin contains an upper Miocene-Pleistocene continental sequence with lignite intervals at various stratigraphic levels (van Vugt *et al.* 1998; Steenbrink *et al.* 2006). After an initial Late Miocene–Late Pliocene homogeneous depositional environment controlled by a single long N–S graben, the basin has been split and fragmented into separate sub-basins and depocentres by ENE–WSW normal faults, producing the individual Florina (F), Ptolemais (P) and Servia (S) sub-basins and a complete re-organization of the drainage network (Fig. 13). Alluvial fans emerging from the the N–S range front on the west side of the Florina basin show continuous profiles and undisturbed surfaces across the range-bounding fault, suggesting their tectonic quiescence. The flat floor of the Florina basin lies undisturbed at ∼600 m a.s.l. and headward drainage incision from the Vardar river catchments is currently halted at the eastern margin of the basin (Fig. 15). The northward direction of flow once the river has exited the Florina basin contrasts with the general southward flow of the large Vardar catchment. The change in sedimentation pattern and the history of sub-basin fragmentation constrain the inception of the ENE–WSW fault system to between Late Pliocene and Early Pleistocene (Pavlides & Mountrakis 1987; Metaxas *et al.* 2007). Incision of Neogene marls and overlying Pleistocene conglomerates at the southern end of the Florina basin, whose deposition was controlled by the activity of the N–S range-front fault (IGME 1981, 1987, 1990, 1997), and of the former depositional surface of the basin itself, indicates progressive uplift and backtilting in the footwall of the NE–SW Xino Nero Fault and reduction in the activity of the main N-S fault (Figs 15 and 16). The drainage

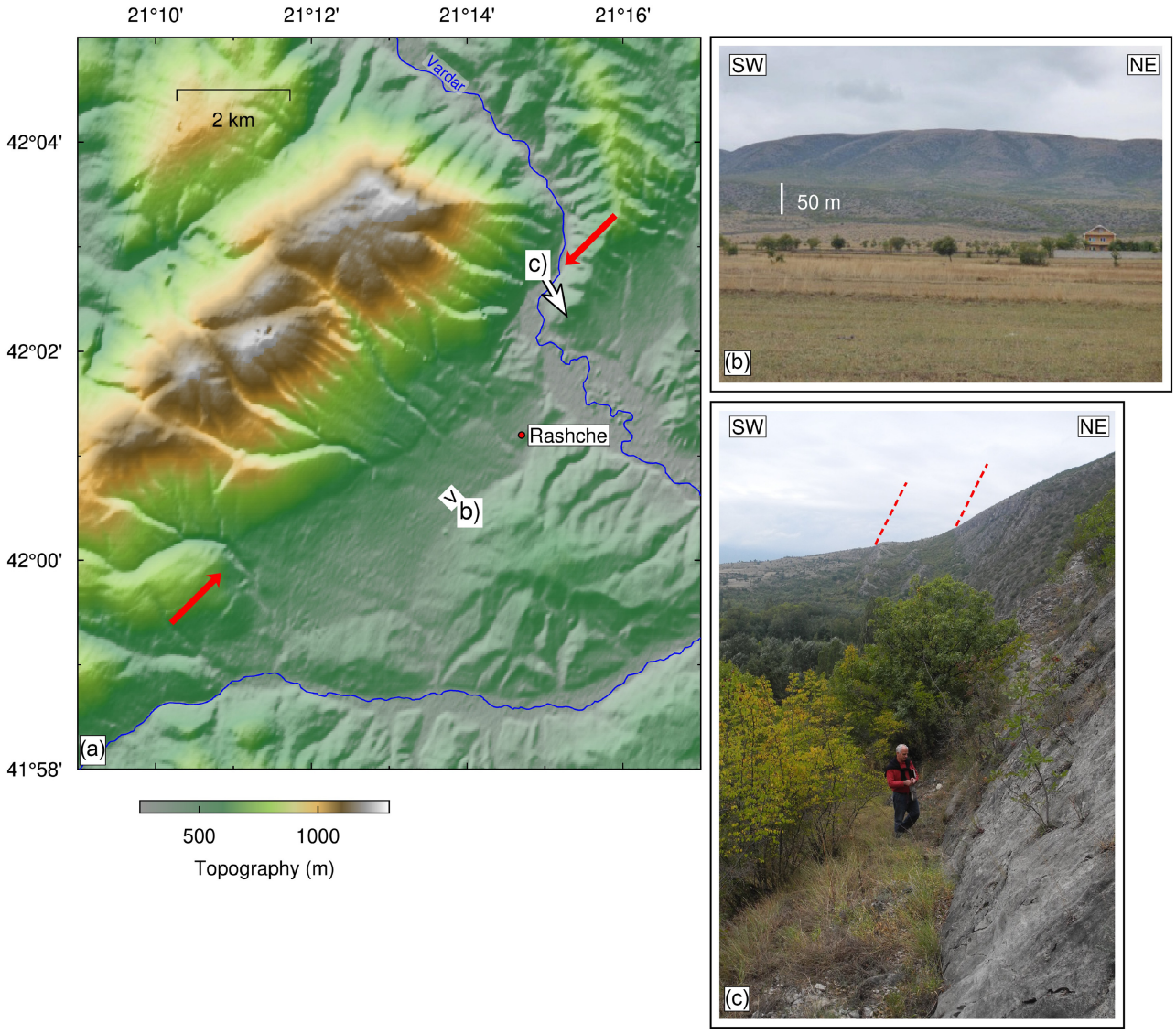

Figure 12. (a) AW3D30 ALOS DEM and the active normal fault near Rashche, between the red arrows. (b) View over the Rashche fault taken from 42.0110°N, 21.2316°E. (c) View over the Rashche fault and cumulative offset across the scarp. Picture taken from 42.0453°N, 21.2488°E.

divide between the Florina and Ptolemais basins (Fig. 16) now runs parallel to the Xino-Nero fault, within the Neogene and Quaternary sands and conglomerates whose deposition was previously controlled by the Bitola-Florina fault.

We extend previous observations on the relation between the ~N–S and ~E–W fault systems (Pavlides & Mountrakis 1987; Goldsworthy *et al.* 2002) by highlighting an abandoned meander system cutting through the current drainage divide between the Florina and Ptolemais sub-basins (Fig. 15). This abandoned drainage system confirms the former continuity of the N–S drainage network across the Florina and Ptolemais sub-basins. The relict meander (Figs 15b and c) probably represents the last phase of drainage continuity between the two basins, incising through the lowest elevation along the ridge separating them, leaving what is now a dry 'wind gap'. Communication between the two basins, and the axial drainage system itself, was presumably abandoned through progressive uplift and tilting of the footwall of the Xino–Nero fault (Fig. 16), whose activity has determined the internal drainage of the Ptolemais basin (Fig. 13b).

Several bedrock fault scarps outcropping at the base of the fault-controlled range fronts in the Ptolomeis basin indicate recent activity of the ENE-WSW oriented normal faults (Pavlides & Mountrakis 1986, 1987; Goldsworthy *et al.* 2002). Slip-vector directions measured on the fault scarps are similar to those in nearby well-constrained fault-plane solutions and geodetic extension axes from the GPS velocity field (Figs 4 and 15), all consistent with an NW–SE extension direction.

The evolution of the FPS basin provides the clearest geomorphological expression of the change in strike of active normal faulting that has been repeatedly observed elsewhere in NW Greece, South Albania and the Republic of Northern Macedonia, the timing of which is poorly constrained between Late Pliocene and Pleistocene (Pavlides & Mountrakis 1987; Mercier *et al.* 1989; Burchfiel *et al.* 2000; Goldsworthy *et al.* 2002; Burchfiel *et al.* 2008). Inception of activity on the ~NE–SW fault system in northern Greece is broadly simultaneous with the draining of the great Pliocene lake system formed by interconnected basins that occupied more than 80 per cent of the present-day North Macedonia (Dumurdzanov *et al.* 2005).

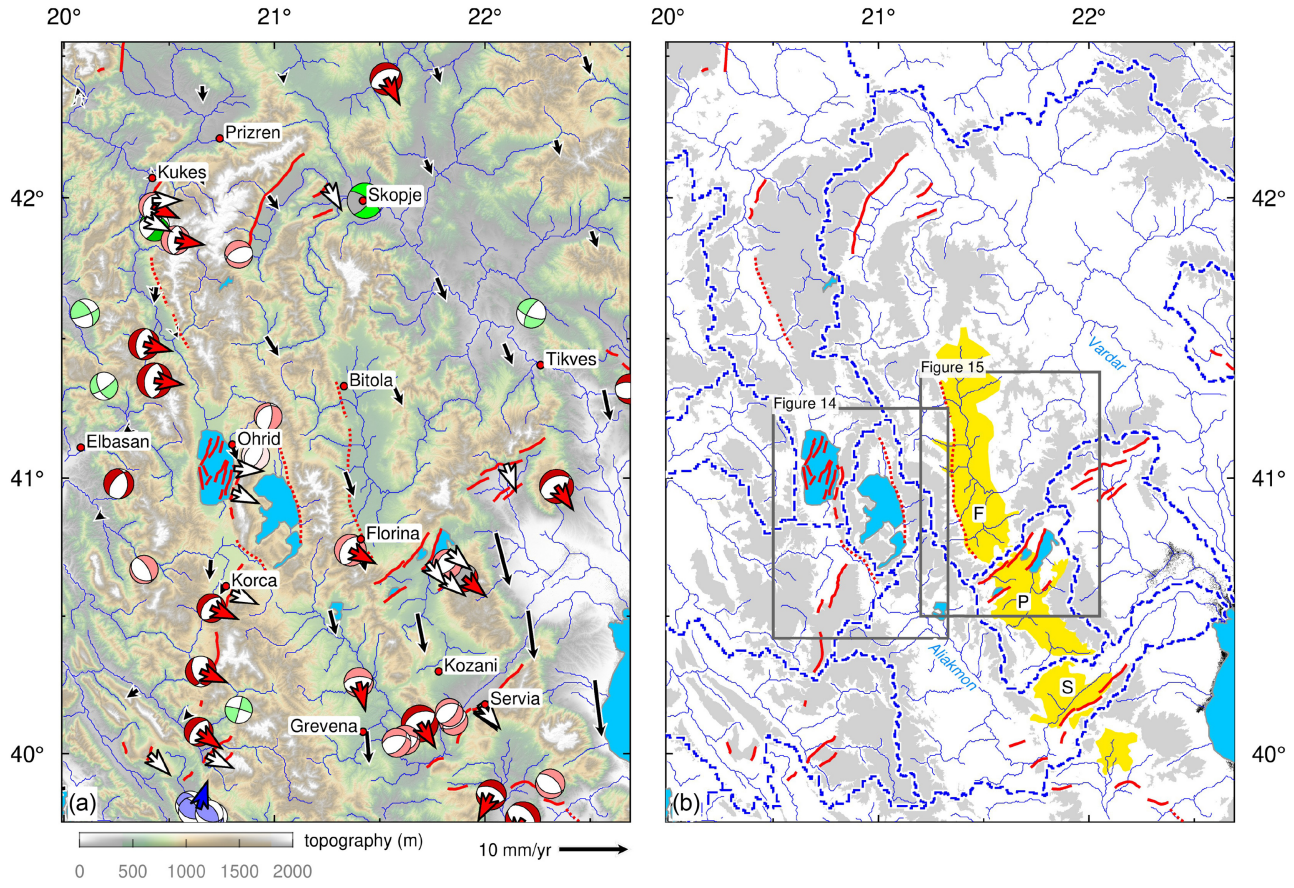

Figure 13. Overview of the active faulting and drainage patterns in the highest part of the Western Balkans and around the Florina(S)-Ptolemais(P)-Servia(S) basin system. (a) AW3D30 ALOS DEM and main fault systems (red continuous lines if active, dashed if inactive), GPS velocities (black arrows, relative to Eurasia). Blue dashed lines show the divides of the main drainage catchments resulting from the fragmentation of the FPS basin by ENE-WSW trending normal faults. (b) Same as (a) with topographic elevations above 1000 m shown in gray and deposits of the FPS basin emphasized in yellow. Grey boxes outline the areas of Figs 14 and 15.

That enclosed and partly interconnected internal drainage system formed a series of lakes separated by a low sill from the Aegean domain near Tikves (Fig. 13; Dumurdzanov *et al.* 2005; Burchfiel *et al.* 2008). During Pleistocene time, the sill was breached and the Vardar River and its drainage system developed by rapid headward erosion. Capture and incision by the Vardar River and its tributaries removed a large volume of Pleistocene and older sediments from the central Macedonian basins (Dumurdzanov *et al.* 2005), but incision has not yet reached the more distant basins, such as Bitola-Florina (Fig. 13) and Tetovo (Fig. 10). The present-day drainage system results from the competition between regional drainage integration by the Vardar catchment and activity on ∼NE–SW normal faults which, by disrupting the earlier basin configuration (i.e. FPS basin) controlled by ∼N–S normal faults, has been locally successful in establishing new catchment boundaries (e.g. Ptolemais basin in Fig. 13).

5.6 Thessaly and the 2021 earthquake sequence

Quaternary and active faulting in Thessaly has been studied extensively by Caputo & Pavlides (1993) and Caputo *et al.* (1994, 2021). Regional morphology is dominated by two large NW–SE sedimentary basins (Larissa and Karditsa; Figs 1 and 17) and their bounding ridges (the Pindos range, Central Hills and Olympos–Ossa–Pilion range) formed in response to NE-SW extension. According to Caputo & Pavlides (1993), the extension direction has recently (Middle Pleistocene) changed from NE–SW to N–S. The younger normal faults, striking approximately E–W to ESE–WNW, form graben that cross-cut the older structures, uplifting and offsetting Late Quaternary deposits in a pattern that continues south into central mainland Greece and is confirmed by the focal mechanisms of both large earthquakes (Fig. 2) and microearthquakes (Hatzfeld 1999). In Thessaly, the ESE-WNW trending active faulting is concentrated into northern (39.5–40.0° N) and southern (39.0–39.5° N) zones (Caputo & Pavlides 1993; Caputo 1995; Goldsworthy *et al.* 2002) (Figs 2 and 17). The southern zone was the most seismically active in modern times (Ambraseys & Jackson 1990), until a sequence of three events (M_w 6.2, 6.0, 5.3) occurred in March 2021 in the northern zone (Fig. 17), containing faults (Tyrnavos, Larissa, Gyrtoni, Vlachogianni and Rodia Faults) that are both south and north-dipping, slightly oblique to the main NW-SE morphological trend, and generally display small cumulative displacements.

The 2021 earthquakes confirm the continuation to the NW of the northern Thessaly zone of NNE–SSW extension, reaching close to the Ptolomeis–Servia fault systems (Fig. 17a). The lack of substantial co-seismic surface faulting in those earthquakes and the discordance between their fault locations determined by InSAR and the local topography (Ganas *et al.* 2021; Tolomei *et al.* 2021) suggest that the responsible faults are in a relatively early stage of development. We therefore interpret this 2021 sequence as indicating the NW propagation of a newly established fault system more clearly

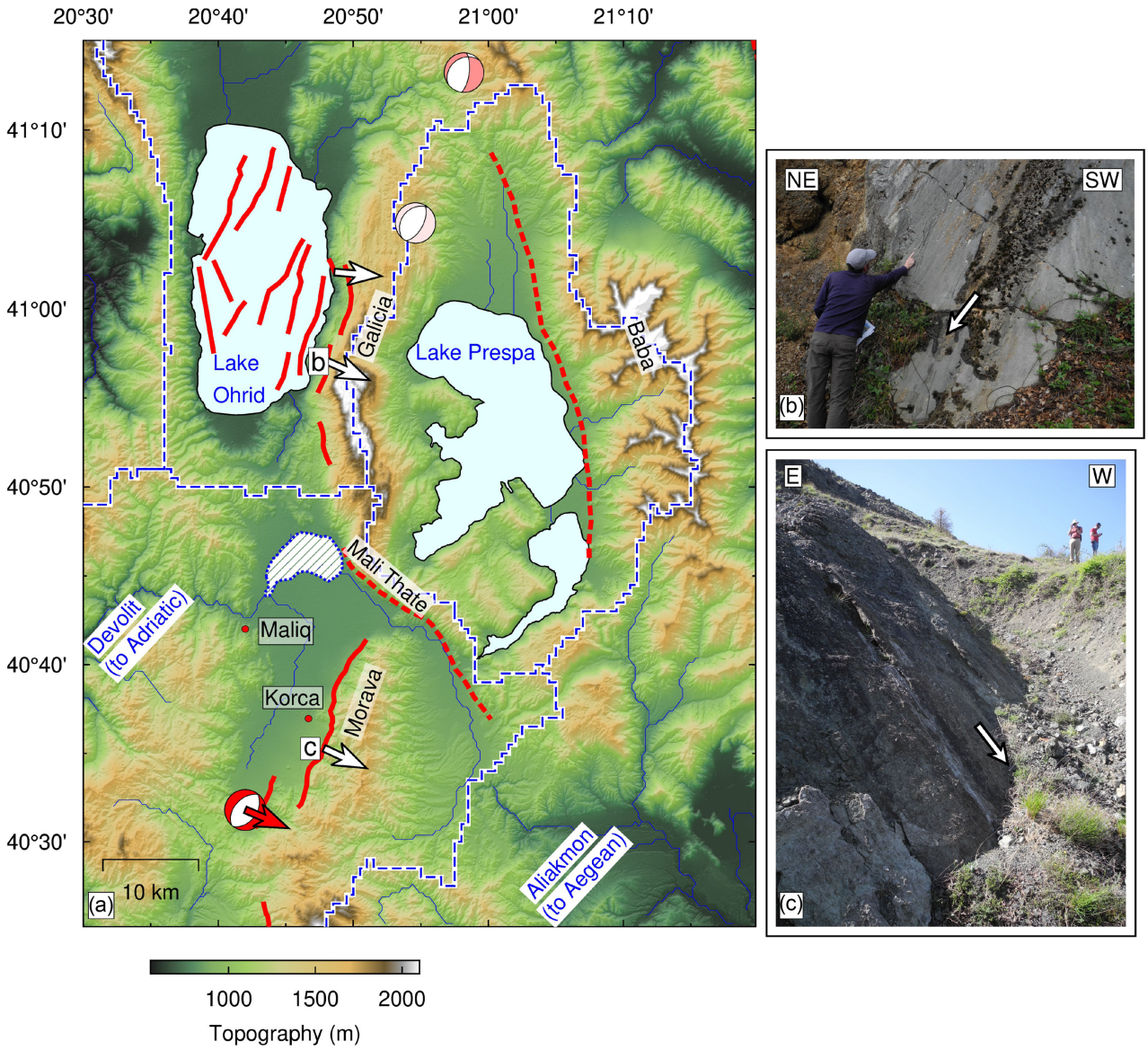

Figure 14. (a) AW3D30 ALOS DEM and evidence for active normal faulting near Korca and Lake Ohrid. Inferred active faults are marked by continuous red lines and dashed when activity is uncertain. Active faults in Lake Ohrid from Lindhorst *et al.* (2015). The white and red arrows indicate the directions of the slip vector measured on striated fault surfaces and from body-wave modelling, respectively. The large dashed blue line shows the regional drainage divide between Adriatic and Aegean Seas, as well as the internal drainage basin of the Prespa lakes. Oblique hatched pattern shows the area occupied by Lake Maliq in historical times (Dufaure *et al.* 1999), indicative of active tectonic subsidence between Korca and Lake Ohrid. (b) Striated fault surface on the fault system bounding Lake Ohrid to the east (40.9522°N, 20.7999°E). (b) Striated fault surface along the Korca fault bounding the Morava mountain (40.5903°N, 20.7975°E).

expressed to the SE by the Larissa, Gyrtoni, Rodia and Tyrnavos fault segments.

The Servia-north Thessaly region, therefore, like the Ohrid–Prespa–Bitola–Florina region, is one in which the direction of active extension changes over a relatively short distance, seen in both the orientation of active faulting and in the GPS strain rates (Fig. 17c), but $\Delta\dot{A}_n$ remaines $<$ or ≈ 1, implying that, locally, the extension occurs in only one direction. In both places the spatial and temporal changes in faulting have had a profound effect on the drainage systems, and in the case of Thessaly, are likely to lead to the integration of the formerly separated Karditsa and Larissa basins (Caputo *et al.* 1994, 2021).

6 DISCUSSION

6.1 Relationship between faulting and the dynamic controls on the regional velocity field

Based on the above observations and analyses, the regional kinematics of the southwestern Balkans in a Eurasian reference frame can be summarized as:

(1) Seaward, roughly westward, motion of the Albanides–Hellenides mountains. This motion occurs from 39° to 43°N and is characterized by extension in the highlands and shortening along the coastal belt of Albania and northern Greece (Copley *et al.* 2009; D'Agostino *et al.* 2020).

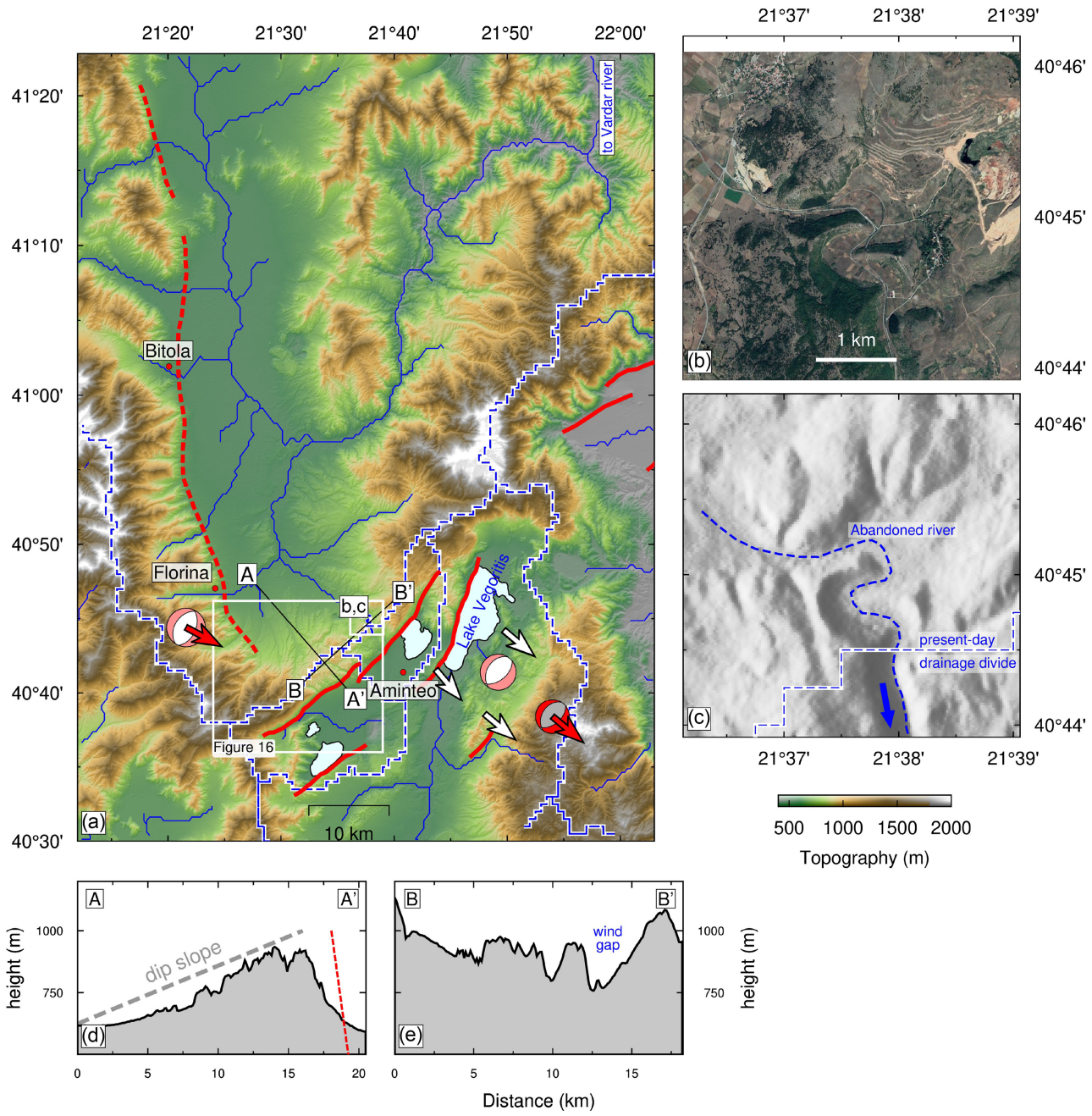

Figure 15. Morphology and active faults of the Florina(S)–Ptolemais basin system. (a) AW3D30 ALOS DEM and trace of the main faults (in red, continuous when active, dashed if inactive). The blue dashed line shows the divide between the Florina and Ptolemais basins resulting from the activity of the ENE–WSW trending normal faults. Zoomed Google Earth and topographic images in (b) and (c) show a detailed view of the abandoned course of the drainage system connecting the Florina and Ptolemais basins. Topographic profiles perpendicular (d) and parallel (e) to the ENE–WSW trending active normal fault.

(2) Motion of the internal part of the Balkans roughly southwards towards the Hellenic subduction zone, which is part of the larger-scale motion of the entire Aegean and western Anatolia (McKenzie 1972; McClusky *et al.* 2000).

Our region of study occupies part of each of these kinematic patterns, and the junctions between them. A characteristic of the region is that the patterns of faulting have evolved through time.

Previous work has demonstrated that lateral variations in GPE arising from crustal thickness contrasts play an important role in governing the deformation. The subparallel thrust and normal faults in western and central Albania have been attributed to the forces arising from the elevation contrast between central Albania and the interior of the Adriatic (Copley *et al.* 2009; Métois *et al.* 2015; D'Agostino *et al.* 2020). If the Adriatic has become weaker through time, for example because of the deposition of a thick blanket of insulating sediment, then a reduction in the heights of mountains that can be supported, and accompanying normal-faulting in the high ground, can result (Copley *et al.* 2009). On a wider scale, the motion of central Greece, the Aegean and western Anatolia towards the Hellenic subduction zone has also been attributed to lateral variations in GPE (e.g. McKenzie 1972; England *et al.* 2016). In this case, the tractions transmitted across the interface between the

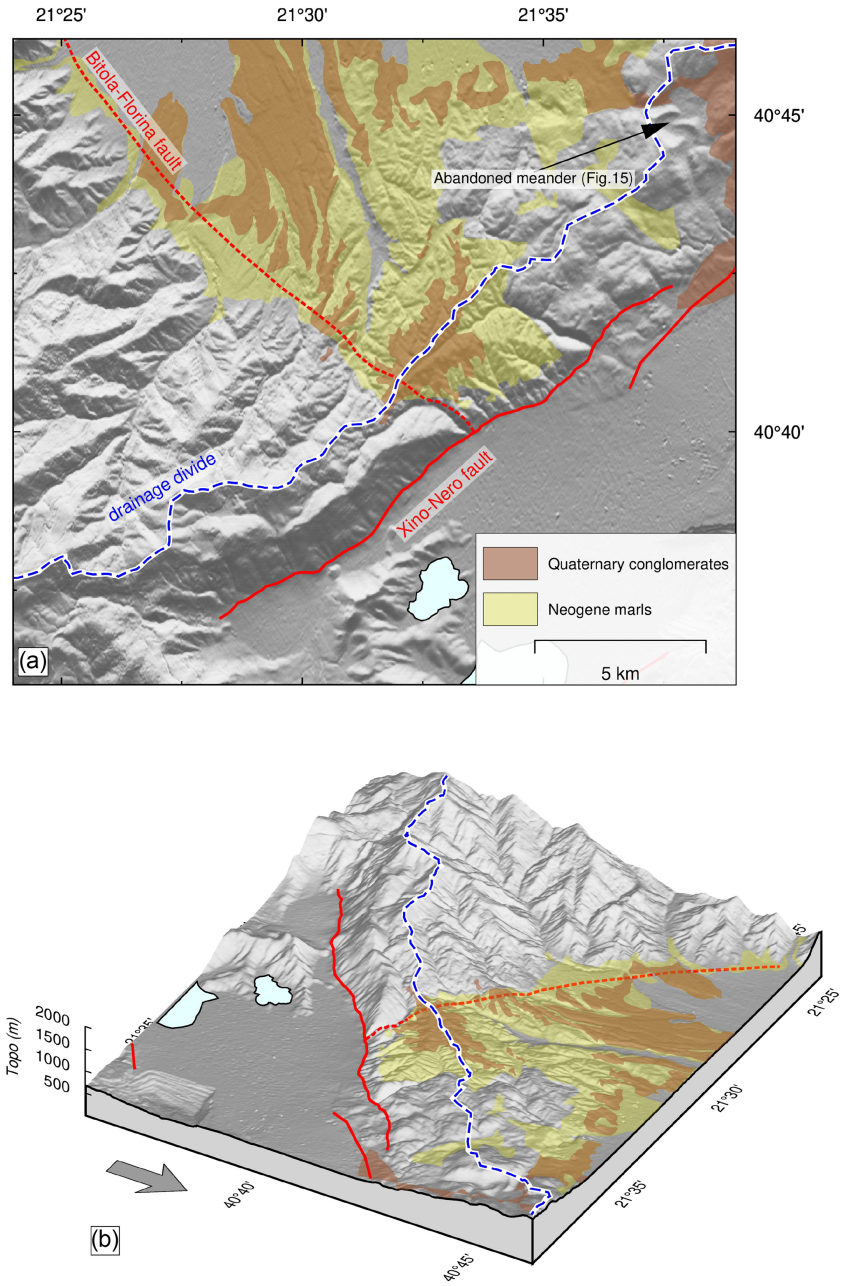

Figure 16. (a) Map and (b) perspective diagram of the topography and Quaternary geology at the southern margin of the Florina basin. Incision of Neogene fluvial/lacustrine deposits and Quaternary conglomerates at the top of the infill of the Florina basin, suggests footwall uplift of the Xino–Nero fault and deactivation of the Florina range-bounding fault, locally covered by the uninterrupted slopes and apexes of the alluvial fans. Geological boundaries in the footwall of the Xino–Nero fault have been digitised from IGME (1981, 1990).

subducting Mediterranean oceanic lithosphere and the over-riding continental lithosphere of the Aegean limit the GPE contrasts that can be sustained. The cessation of extension in the central-south Aegean (Sea of Crete) in the Late Miocene (e.g. Jolivet and Brun, 2010) implies that the crustal thickness in that region is in force balance with the tractions transmitted across the subduction interface. Active extension now occurs in the regions surrounding the Aegean Sea, in central Greece and western Turkey, where there are present-day crustal-thickness gradients (e.g. Sodoudi *et al.* 2006; Aktug *et al.* 2009; Floyd *et al.* 2010). Our inferences described above of the northwards propagation of NE–SW to E–W striking extensional fault systems, overprinting prior N–S systems, is consistent with this kinematic situation.

Such a configuration is analogous to that in mountain belts, where crustal thickening occurs until the GPE contrast between the mountains and adjacent lowlands reaches the maximum level that can be supported by the forces transmitted across the boundary between them, at which time shortening becomes focused on the margins of the belt, and a plateau is formed (e.g. Molnar & Lyon-Caen 1988). The equivalent extensional configuration would be thin crust, surrounded by thicker crust, with the extension focused on the gradient between them, as seen in the Aegean (fig. 11 in Floyd *et al.* 2010).

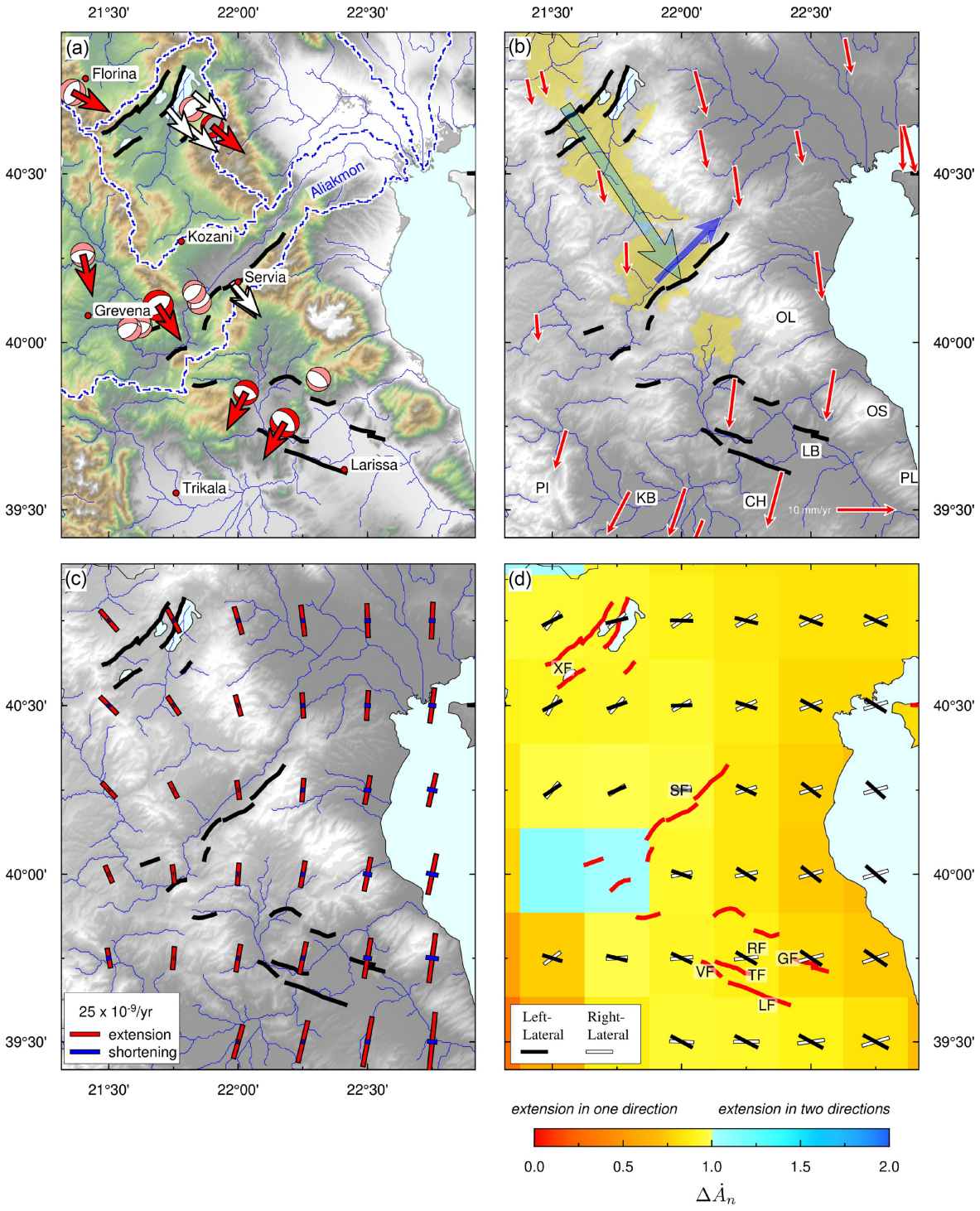

Figure 17. (a) Morphology and active faults in Thessaly and Macedonia. Focal mechanisms and slip vectors follow the earlier conventions. (b) GPS velocities relative to Eurasia. Deposits of the FPS basin are emphasized in yellow. The shaded large blue vectors indicate the former drainage through the FPS disrupted by the present course of the Alkiamon river (smaller blue arrow). Geographic features: OL—Mount Olympos; Pi—Pindos Range; KB—Karditsa basin; LB—Larissa basin; CH—Central Hills; OS—Ossa Mountain and PL—Pilion Mountain. (c) Principal axes of the strain-rate field. (d) Directions of no-length-change and coloured value of $\Delta\dot{A}_n$ (as in Fig. 4b). Faults (in red): GF—Gyrtoni; LF—Larissa; RF—Rodia; SF—Servia; TY—Tyrnavos; VF—Vlachogianni and XF—Xino Nero.

As the outwards migration of extension related to the force balance in the Hellenic Trench has occurred within our study region, normal faulting with slip vectors oriented mostly N–S (central Greece) to NW–SE (northern Greece) has become juxtaposed with the ∼E–W extension related to the GPE contrast between the Albanides–Hellenides and the Adriatic. The nature of the faulting in this region of juxtaposition can provide insights into the relationship between the regional dynamics and the accommodation of strain in the brittle and ductile parts of the lithosphere. Previous work in the forelands of mountain belts, regarding the relationship

between the seismogenic thickness, the effective elastic thickness and the thermal structure of the lithosphere, implies that in those settings the majority of the force transmitted through the lithosphere is supported in the brittle seismogenic layer (e.g. Maggi *et al.* 2000; Copley *et al.* 2011; Jackson *et al.* 2021, and references therein). In that situation, the geometry and rheology of the faulting dominate the deformation that results from a given distribution of forces. By contrast, some other continental regions deform pervasively over large horizontal length-scales of hundreds to thousands of kilometres, and have a strain distribution that implies quasi-continuous behaviour at those length-scales (e.g. England & Molnar 1997; Flesch *et al.* 2001). In certain regions, such as SW Turkey where the strain-rate field has the property $\Delta\dot{A}_n > 1$, the deformation cannot be accommodated by a stable configuration of faulting, resulting in a complex and unstable fault network (e.g. Howell *et al.* 2017). In such cases, the necessary continual rearrangement of the faulting implies that the deeper ductile layer controls the dynamics of the region, and the brittle faulting in the upper crust must evolve through time to accommodate the velocity field imposed upon it from beneath. These two contrasting styles of behaviour are to be expected: a fault-dominated force balance where the seismogenic layer is thick and earthquake stress drops can be relatively large, and a ductile-dominated rheology where the seismogenic layer is thin, and large velocity gradients within the ductile layer impose significant tractions on the base of upper-crustal blocks. An extension of this logic is that the long-running dispute, regarding whether to view continental deformation in general (e.g. England & Molnar 1997; Thatcher 2009), and that of the Aegean in particular (e.g. McClusky *et al.* 2000; Floyd *et al.* 2010), as the behaviour of a continuum or of 'micro-plates', is also an entirely location- and scale-dependent discussion, relating to the thickness and rheology of the brittle and ductile parts of the lithosphere, and therefore the dominant controls on the force balance.

Our observations show that the region in eastern Albania, southern North Macedonia and northern Greece, where the extension related to the Albania-Adriatic GPE contrast and that related to the larger-scale motion towards the Hellenic Trench are juxtaposed, falls into an intermediate category between the end-members discussed above (of an entirely brittle- or ductile-dominated force balance). The large-scale motion towards the Hellenic Trench, involving a progressive increase in velocity over a length-scale of over 500 km and multiple active fault systems, implies a significant ductile influence on the motions, rather than brittle faulting accommodating the necessary strain onto a small number of localized (weakest) fault systems. However, in the Florina–Ptolemais–Servia region of northern Greece and southern North Macedonia, NE–SW faults have offset the N–S faulting related to the extension in Albania, and the geomorphology implies that the N–S striking faults have become inactive (Figs 13–16). Rather than the situation seen in SW Turkey, where $\Delta\dot{A}_n > 1$ and extension with two horizontal principal axes is accommodated by complex faulting with multiple slip-vector orientations (Howell *et al.* 2017), our study region is characterized by two spatially distinct regions of extension, $\Delta\dot{A}_n \leq 1$ and a consistent slip-vector orientation within each one (Fig. 3). Furthermore, the fault strikes are consistent with the directions of no-length-change shown in Fig. 4(b). Such a configuration implies that, superimposed upon the large-scale flow towards the Hellenic Trench that sets the far-field motions, within this region individual fault systems play a role in controlling the kinematics—one set of extensional faults offsets the other and then determines the location of each extensional regime, rather than the faulting being unstable and characterized by multiple slip-vector orientations in response to an underlying velocity field with two extensional principal axes. This combined influence, of far-field forces transmitted through the ductile layer and local brittle controls on the location and nature of domains of faulting, represents a situation that is likely to be widespread. This situation has been revealed in our study area by our new observations, enabled by the local geology and the geomorphology it creates when undergoing faulting (e.g. resistant limestone fault-bounded topography and preserved fault planes), but is also likely to occur in other regions that are less amenable to such analyses. The spatial consistency of earthquake slip vectors over most regions of distributed continental deformation (e.g. Fig. 3; Molnar & Lyon-Caen 1989; Taymaz *et al.* 1991; Jackson *et al.* 1992; Talebian & Jackson 2004; Wimpenny *et al.* 2018) shows that the pattern described in SW Turkey by Howell *et al.* (2017) is unusual. There is no reason, on the basis of the dynamics of the ductile part of the lithosphere, why the active strain should not have two horizontal compressional or extensional principal axes (e.g. Houseman & England 1986; Flesch *et al.* 2001). The rarity of this configuration therefore implies that the force balance in the brittle upper crust, and the energetically unfavourable situation of constructing an unstable and temporally evolving fault network, plays a role alongside the distributed deformation of the ductile crust and mantle in controlling the kinematics of distributed deformation belts. This logic further emphasizes the unhelpful nature of taking a purely continuum or purely micro-plate approach to viewing continental deformation.

6.2 Evolution within fault systems

As explained in the Introduction, a change in the orientation of the overall strain-rate field with time, or rotations of fault-bounded blocks about vertical axes within an unchanging overall strain-rate field, will mean that the faulting will have to adapt with time, in order for the fault strikes to follow the no-length-change directions in the velocity field. Any changes to the strain-rate field and the rotations, if they occur, are likely to be gradual, rather than sudden. But what is clear from the geology and geomorphology is that any resulting changes to the faulting are not gradual, with constantly appearing new faults, each with a different strike and moving a small amount before being replaced by its successor. Instead, the landscape and geological record are always dominated by large finite offsets on a small number of discrete fault sets that take up the motion, suggesting that there is a trade-off between continuing to move faults that are no longer perfectly aligned for the velocity field, and creating new ones. In the Ohrid–Prespa region, the discordance between the Ohrid and Korca faults is about 30° (Fig. 14). Between the Florina-Bitola and Xino Nero faults it about 45° (Fig. 15), and in Thessaly it is about 30° between the youngest faults and the NW–SE older faults bounding the Karditsa and Larissa basins (Fig. 17). Further south, in southern Thessaly, Locris (∼38.5N 23.0E) and the Megara basin of the eastern Gulf of Corinth (∼38.0N 23.0E) the discordance between currently-active and now-inactive older Neogene faults is again in the range 30°–45° (Caputo & Pavlides 1993; Goldsworthy *et al.* 2002). The implication is that the faults need to become unfavourably aligned by about 30°–40° before they become inactive and a new set forms that is favourably aligned. Remarkably, the same range and effect is observed seaward of oceanic trenches, where swath bathymetry mapping of the outer rises has shown that normal faults generated by flexure are generally parallel to the trenches. Where the angle between the trench axis and the fabric within the oceanic plate generated at the ridge axis where it formed is less than about 30°, normal faults generally follow that

inherited fabric. But where that angle is greater than about 30°, flexure forms new faults whose strike is controlled by that of the trench axis, rather than by the inherited ridge-generated fabric (e.g. Masson 1991; Mortera-Gutiarrez *et al.* 2003). The consistency of these observations, together with the relatively narrow range of nearly all observed earthquake stress drops, and (where it is possible to do so) the estimated shear stresses on faults when they fail, all point to the conclusion that the rheology of seismogenic faults is much the same everywhere, and that the variety of geological manifestations of such faulting, such as the wavelength and amplitude of topography they generate, is more a matter of how those limiting stresses are supported by a seismogenic layer of varying thickness (e.g. Foster & Nimmo 1996; Copley & Woodcock 2016).

7 CONCLUSIONS

The exceptional quality, quantity and variety of observational data related to Late Quaternary tectonics in the western Balkans allow an unusual level of detail to be seen in kinematic patterns of deformation active today, and how they have evolved over the last few million years. This in turn allows insights into the processes that influence that deformation, and how they interact. In particular, the evolution of drainage systems and their associated geomorphology reveal a history that could not easily be established by more conventional stratigraphic evidence. Most regions of currently active continental tectonics do not have the richness of evidence seen in the western Balkans, but the processes revealed in this study are quite general and there is no reason to doubt that they, and their interplay, are not also operating in other areas where the available data are more sparse. This study once again emphasizes the advantages of looking at places that are deforming today: it is inconceivable that the necessary exposure or resolution in time and space would be possible in old, inactive mountain belts.

ACKNOWLEDGMENTS

We thank IGME (Hellenic Geological Service) and Thanassis Ganas for making available geological maps. ALOS AW3D30 topographic data have been downloaded at https://www.eorc.jaxa.jp/ALOS/en/aw3d30/index.htm. Drainage network and hydrographic catchments have been extracted from the HydroSHEDS data set available at https://www.hydrosheds.org. ND acknowledges support from MAE (Ministero Affari Esteri) Funding (Progetti Grande Rilevanza 2019). AC and JJ were partly supported by the NERC grant 'Looking Inside the Continents from Space'. This work was also partly supported by COMET, which is the NERC Centre for the Observation and Modelling of Earthquakes, Volcanoes and Tectonics, a partnership between UK Universities and the British Geological Survey. Figures were produced with the GMT software package (Wessel *et al.* 2019). We are grateful to the editor (Kosuke Heki) and to reviewers Riccardo Caputo and Philip England for their constructive comments.

DATA AVAILABILITY

The authors confirm that the data supporting the findings of this study are available within the paper or its Supporting Information.

REFERENCES

Aktug, B. *et al.*, 2009. Deformation of Western Turkey from a combination of permanent and campaign GPS data: limits to block-like behavior, *J. geophys. Res.: Solid Earth,* **114**(B10).

Ambraseys, N., 2009. *Earthquakes in the Mediterranean and Middle East: A Multidisciplinary Study of Seismicity up to 1900,* Cambridge University Press.

Ambraseys, N. N. & Jackson, J. A., 1990. Seismicity and associated strain of central Greece between 1890 and 1988, *Geophys. J. Int.,* **101**(3), 663–708.

Anderson, H. & Jackson, J., 1987. Active tectonics of the Adriatic region, *Geophys. J. Int.,* **91**(3), 937–983.

Argnani, A., 2013. The influence of Mesozoic palaeogeography on the variations in structural style along the front of the Albanide thrust-and-fold belt, *Ital. J. Geosci. (Boll. Soc. Geol. It.),* **132**(2), 175–185.

Arizaga, I., Barchi, M., Fantoni, R. & Storer, P., 2017. Reconstruction of the Periadriatic Mesozoic Platforms through reflection seismic profiles and deep exploratory wells, *J. Med. Earth Sci.,* **9,** 81–85.

Armijo, R., Meyer, B., King, G. C. P., Rigo, A. & Papanastassiou, D., 1996. Quaternary evolution of the Corinth Rift and its implications for the Late Cenozoic evolution of the Aegean, *Geophys. J. Int.,* **126**(1), 11–53.

Asano, Y., Saito, T., Ito, Y., Shiomi, K., Hirose, H., Matsumoto, T., Aoi, S., Hori, S. & Sekiguchi, S., 2011. Spatial distribution and focal mechanisms of aftershocks of the 2011 off the pacific coast of tohoku earthquake, *Earth Planets Space,* **63**(7), 29, doi:10.5047/eps.2011.06.016.

Baker, C., Hatzfeld, D., Lyon-Caen, H., Papadimitriou, E. & Rigo, A., 1997. Earthquake mechanisms of the Adriatic Sea and Western Greece: implications for the oceanic subduction-continental collision transition, *Geophys. J. Int.,* **131**(3), 559–594.

Bega, Z., 2015. Hydrocarbon exploration potential of Montenegro—a brief review, *J. Petrol. Geol.,* **38**(3), 317–330.

Bega, Z. & Schleder, Z., April 4, 2017 Tuesday, AAPG Annual Convention and Exhibition, Houston, Texas, 2017. *Review of Mesozoic Exploration Plays in the Montenegro - NW Albania Segment of South Adriatic Basin*.

Bega, Z. & Soto, J., 2017. The Ionian Fold-and-Thrust Belt in Central and Southern Albania: a petroleum province with triassic evaporites, in *Permo-Triassic Salt Provinces of Europe, North Africa and the Atlantic Margins,* pp. 517–539, eds Soto, J. I., Flinch, J. F. & Tari, G., Elsevier.

Benetatos, C. & Kiratzi, A., 2006. Finite-fault slip models for the 15 April 1979 (Mw 7.1) Montenegro earthquake and its strongest aftershock of 24 May 1979 (Mw 6.2), *Tectonophysics,* **421**(1), 129–143.

Berberian, M., Jackson, J. A., Qorashi, M., Talebian, M., Khatib, M. & Priestley, K., 2000. The 1994 Sefidabeh earthquakes in eastern Iran: blind thrusting and bedding-plane slip on a growing anticline, and active tectonics of the Sistan suture zone, *Geophys. J. Int.,* **142**(2), 283–299.

Biermanns, P., Schmitz, B., Mechernich, S., Weismüller, C., Onuzi, K., Ustaszewski, K. & Reicherter, K., 2022. Aegean-style extensional deformation in the contractional southern Dinarides: incipient normal fault scarps in Montenegro, *Solid Earth,* **13**(6), 957–974.

Briole, P., Ganas, A., Elias, P. & Dimitrov, D., 2021. The GPS velocity field of the Aegean. New observations, contribution of the earthquakes, crustal blocks model, *Geophys. J. Int.,* **226**(1), 468–492.

Burchfiel, B., King, R., Todosov, A., Kotzev, V., Durmurdzanov, N., Serafimovski, T. & Nurce, B., 2006. GPS results for Macedonia and its importance for the tectonics of the Southern Balkan extensional regime, *Tectonophysics,* **413**(3), 239–248.

Burchfiel, B. *et al.*, 2008. Evolution and dynamics of the Cenozoic tectonics of the South Balkan extensional system, *Geosphere,* **4**(6), 919, doi:10.1130/GES00169.1.

Burchfiel, C. B., Nakov, R., Tzankov, T. & Royden, L. H., 2000. Cenozoic Extension in Bulgaria and Northern Greece: the Northern Part of the Aegean Extensional Regime, *Geol. Soc. Lond. Spec. Publ.,* **173**(1), 325–352.

Caputo, R., 1995. Inference of a seismic gap from geological data: Thessaly (central greece) as a case study., *Ann. Geophys.,* **38**(1), 1–19.

Caputo, R. & Pavlides, S., 1993. Late Cainozoic geodynamic evolution of Thessaly and surroundings (central-northern Greece), *Tectonophysics,* **223**(3), 339–362.

Caputo, R. & Pavlides, S., 2013. *Greek Database of Seismogenic Sources,version 2.0.0: A compilation of potential seismogenic sources (Mw > 5.5) in the Aegean Region,* http://gredass.unife.it (Access date: July 20th, 2022).

Caputo, R., Bravard, J.-P. & Helly, B., 1994. The Pliocene-Quaternary tectosedimentary evolution of the Larissa Plain (Eastern Thessaly, Greece), *Geod. Acta,* **7**(4), 219–231.

Caputo, R., Monaco, C. & Tortorici, L., 2006. Multiseismic cycle deformation rates from Holocene normal fault scarps on Crete (Greece), *Terra Nova,* **18**(3), 181–190.

Caputo, R., Catalano, S., Monaco, C., Romagnoli, G., Tortorici, G. & Tortorici, L., 2010. Active faulting on the island of Crete (Greece), *Geophys. J. Int.,* **183**(1), 111–126.

Caputo, R., Helly, B., Rapti, D. & Valkaniotis, S., 2021. Late Quaternary hydrographic evolution in Thessaly (Central Greece): the crucial role of the Piniada Valley, *Quat. Int.,* doi:10.1016/j.quaint.2021.02.013.

Chapman, C., 1978. A new method for computing synthetic seismograms, *Geophys. J. R. astr. Soc.,* **54,** 481–518.

Clarke, P. J. *et al.*, 1997. Geodetic estimate of seismic hazard in the Gulf of Korinthos, *Geophys. Res. Lett.,* **24**(11), 1303–1306.

Copley, A. & Woodcock, N., 2016. Estimates of fault strength from the Variscan foreland of the northern UK, *Earth planet. Sci. Lett.,* **451,** 108–113.

Copley, A., Boait, F., Hollingsworth, J., Jackson, J. & McKenzie, D., 2009. Subparallel thrust and normal faulting in Albania and the roles of gravitational potential energy and rheology contrasts in mountain belts, *J. geophys. Res.: Solid Earth,* **114**(B5), doi:10.1029/2008JB005931.

Copley, A., Avouac, J.-P., Hollingsworth, J. & Leprince, S., 2011. The 2001 Mw 7.6 Bhuj earthquake, low fault friction, and the crustal support of plate driving forces in India, *J. geophys. Res.: Solid Earth,* **116**(B8), doi:10.1029/2010JB008137.

D'Agostino, N., Jackson, J. A., Dramis, F. & Funiciello, R., 2001. Interactions between mantle upwelling, drainage evolution and active normal faulting: an example from the central Apennines (Italy), *Geophys. J. Int.,* **147**(2), 475–497.

D'Agostino, N., England, P., Hunstad, I. & Selvaggi, G., 2014. Gravitational potential energy and active deformation in the apennines, *Earth planet. Sci. Lett.,* **397,** 121–132.

D'Agostino, N. *et al.*, 2020. Active crustal deformation and rotations in the southwestern Balkans from continuous GPS measurements, *Earth planet. Sci. Lett.,* **539,** 116246, doi:10.1016/j.epsl.2020.116246.

Dalmayrac, B. & Molnar, P., 1981. Parallel thrust and normal faulting in peru and constraints on the state of stress, *Earth planet. Sci. Lett.,* **55**(3), 473–481.

Dufaure, J.-J., Fouache, E. & Denèfle, M., 1999. Tectonique et évolution géomorphologique : l'exemple du bassin de Korçë (Albanie)/ Tectonics and geomorphological evolution: the example of the Korçë basin (Albania), *Géomorphologie: Relief, Processus, Environnement,* **5**(2), 111–128.

Dumurdzanov, N., Serafimovski, T. & Burchfiel, B. C., 2005. Cenozoic tectonics of Macedonia and its relation to the South Balkan extensional regime, *Geosphere,* **1**(1), 1–22.

Elezaj, Z., 2009. Cenozoic Molasse Basins in Kosovo and their geodynamic evolution, *Muzeul Olteniei Craiova, Studii şi comunicări. Ştiinţele Naturii,* **25,** 343–350.

Elezaj, Z., 2010. The Neogene of the Dukagjini basin, *Muzeul Olteniei Craiova, Studii şi comunicări. Ştiinţele Naturii,* **26,** 291–295.

England, P. & Molnar, P., 1997. Active deformation of asia: From kinematics to dynamics, *Science,* **278**(5338), 647–650.

England, P., Houseman, G. & Nocquet, J.-M., 2016. Constraints from GPS measurements on the dynamics of deformation in Anatolia and the Aegean, *J. geophys. Res.: Solid Earth,* **121**(12), 8888–8916.

Farías, M., Comte, D., Roecker, S., Carrizo, D. & Pardo, M., 2011. Crustal extensional faulting triggered by the 2010 Chilean earthquake: the Pichilemu Seismic Sequence, *Tectonics,* **30**(6), doi:10.1029/2011TC002888.

Flesch, L. M., Haines, A. J. & Holt, W. E., 2001. Dynamics of the India-Eurasia collision zone, *J. geophys. Res.: Solid Earth,* **106**(B8), 16435–16460.

Floyd, M. *et al.*, 2010. A new velocity field for Greece: implications for the kinematics and dynamics of the Aegean, *J. geophys. Res.: Solid Earth (1978–2012),* **115**(B10), doi:10.1029/2009JB007040.

Foster, A. & Nimmo, F., 1996. Comparisons between the rift systems of east africa, earth and beta regio, venus, *Earth planet. Sci. Lett.,* **143,** 183–195.

Ganas, A., 2020. *Noafaults kmz layer version 3.0 (2020 update),* https://doi.org/10.5281/zenodo.4304613 (Access date: July 20th 2022).

Ganas, A. *et al.*, 2021. Domino-style earthquakes along blind normal faults in northern thessaly (greece): kinematic evidence from field observations, seismology, sar interferometry and gnss, *Bull. geol. Soc. Greece,* **58**(0), doi:10.12681/bgsg.27102.

Geurts, A. H., Cowie, P. A., Duclaux, G., Gawthorpe, R. L., Huismans, R. S., Pedersen, V. K. & Wedmore, L. N. J., 2018. Drainage integration and sediment dispersal in active continental rifts: A numerical modelling study of the central italian apennines, *Basin Res.,* **30**(5), 965–989.

Goldsworthy, M. & Jackson, J., 2000. Active normal fault evolution in greece revealed by geomorphology and drainage patterns, *J. geol. Soc.,* **157**(5), 967–981.

Goldsworthy, M. & Jackson, J., 2001. Migration of activity within normal fault systems: examples from the Quaternary of mainland Greece, *J. Struct. Geol.,* **23**(2), 489–506.

Goldsworthy, M., Jackson, J. & Haines, J., 2002. The continuity of active fault systems in Greece, *Geophys. J. Int.,* **148**(3), 596–618.

Haines, A. & Holt, W., 1993. A procedure for obtaining the complete horizontal motions within zones of distributed deformation from the inversion of strain rate data, *J. geophys. Res.: Solid Earth (1978–2012),* **98**(B7), 12057–12082.

Hancock, P. & Barka, A., 1987. Kinematic indicators on active normal faults in Western Turkey, *J. Struct. Geol.,* **9**(5), 573–584.

Handy, M. R., Giese, J., Schmid, S. M., Pleuger, J., Spakman, W., Onuzi, K. & Ustaszewski, K., 2019. Coupled crust-mantle response to slab tearing, bending, and rollback along the Dinaride-Hellenide Orogen, *Tectonics,* **38**(8), 2803–2828.

Hatzfeld, D., 1999. The present-day tectonics of the aegean as deduced from seismicity, *Geol. Soc. Lond. Spec. Publ.,* **156**(1), 415–426.

Hoffmann, N., 2014. The active tectonic landscape of Lake Ohrid (FYR of Macedonia/Albania), *Ann. Geophys.,* **56**(6), doi:10.4401/ag-6254.

Hoffmann, N., Reicherter, K., Fernández-Steeger, T. & Grützner, C., 2010. Evolution of ancient lake ohrid: a tectonic perspective, *Biogeosciences,* **7**(10), 3377–3386.

Holt, W. & Haines, A., 1993. Velocity fields in deforming Asia from the inversion of earthquake-released strains, *Tectonics,* **12**(1), 1–20.

Houseman, G. & England, P., 1986. Finite strain calculations of continental deformation: 1. method and general results for convergent zones, *J. geophys. Res.: Solid Earth,* **91**(B3), 3651–3663.

Howell, A., Jackson, J., Copley, A., McKenzie, D. & Nissen, E., 2017. Subduction and vertical coastal motions in the eastern Mediterranean, *Geophys. J. Int.,* **211**(1), 593–620.

IGME, 1981. *Geological map of Greece at scale 1:50.000, sheet Vevi*. Institute of Geology and Mineral Exploration, Athens, Greece.

IGME, 1987. *Geological map of Greece at scale 1:50.000, sheet Florina,* Institute of Geology and Mineral Exploration, Athen, Greece.

IGME, 1990. *Geological map of Greece at scale 1:50.000, sheet Kastoria,* Institute of Geology and Mineral Exploration, Athens, Greece.

IGME, 1997. *Geological map of Greece at scale 1:50.000, sheet Ptolemais,* Institute of Geology and Mineral Exploration, Athen, Greece.

IGRS-IFP, 1966. *Étude géologique de l'Epire (Grèce nord—occidentale),* Technip, Paris.

Jackson, J., 1999. Fault death: a perspective from actively deforming regions, *J. Struct. Geol.,* **21**(8), 1003–1010.

Jackson, J., Haines, J. & Holt, W., 1992. The horizontal velocity field in the deforming Aegean Sea region determined from the moment tensors of earthquakes, *J. geophys. Res.: Solid Earth,* **97**(B12), 17657–17684.

Jackson, J., Priestley, K., Allen, M. & Berberian, M., 2002. Active tectonics of the South Caspian Basin, *Geophys. J. Int.,* **148**(2), 214–245.

Jackson, J., McKenzie, D. & Priestley, K., 2021. Relations between earthquake distributions, geological history, tectonics and rheology on the continents, *Phil. Trans. R. Soc. A: Math. Phys. Eng. Sci.,* **379**(2193), 20190412, doi:10.1098/rsta.2019.0412.

Jolivet, L. & Brun, J. P., 2010. Cenozoic geodynamic evolution of the Aegean, *Int. J. Earth Sci. (Geol Rundsch),* **99,** 109–138, doi:10.1007/s00531-008-0366-4.

Kissel, C., Laj, C. & Müller, C., 1985. Tertiary geodynamical evolution of northwestern Greece: paleomagnetic results, *Earth planet. Sci. Lett.,* **72**(2), 190–204.

Kissel, C., Speranza, F. & Milicevic, V., 1995. Paleomagnetism of external southern and central Dinarides and northern Albanides: implications for the Cenozoic activity of the Scutari-Pec Transverse Zone, *J. geophys. Res.: Solid Earth (1978–2012),* **100**(B8), 14999–15007.

Kotzev, K., Nakov, R., Georgiev, T., Burchfiel, B. & King, R., 2006. Crustal motion and strain accumulation in western Bulgaria, *Tectonophysics,* **413**(3), 127–145.

Kumar, A., Mitra, S. & Suresh, G., 2015. Seismotectonics of the eastern Himalayan and indo-burman plate boundary systems, *Tectonics,* **34**(11), 2279–2295.

Le Pichon, X., 1982. Land-locked oceanic basins and continental collision; the Eastern Mediterranean a a case example, in *Mountain Building Processes,* pp. 129–146, ed. K. & H., Academic Press, London.

Lindhorst, K., Krastel, S., Reicherter, K., Stipp, M., Wagner, B. & Schwenk, T., 2015. Sedimentary and tectonic evolution of Lake Ohrid (Macedonia/Albania), *Basin Res.,* **27**(1), 84–101.

Louvari, E., Kiratzi, A. & Papazachos, B., 1999. The Cephalonia Transform Fault and its extension to western Lefkada Island (Greece), *Tectonophysics,* **308**(1), 223–236.

Louvari, E., Kiratzi, A., Papazachos, B. & Hatzidimitriou, P., 2001. Fault-plane solutions determined by waveform modeling confirm tectonic collision in the Eastern Adriatic, *Pure appl. Geophys.,* **158**(9), 1613–1637.

Maggi, A., Jackson, J., McKenzie, D. & Priestley, K., 2000. Earthquake focal depths, effective elastic thickness, and the strength of the continental lithosphere, *Geology,* **28**(6), 495–498.

Masson, D., 1991. Fault patterns at outer trench walls, *Marine Geophys. Res.,* **13,** 209–225.

Mattei, M., D'Agostino, N., Zananiri, I., Kondopoulou, D., Pavlides, S. & Spatharas, V., 2004. Tectonic evolution of fault-bounded continental blocks: comparison of paleomagnetic and GPS data in the Corinth and Megara basins (Greece), *J. geophys. Res.: Solid Earth,* **109**(B2), doi:10.1029/2003JB002506.

McCaffrey, R. & Abers, G., 1988. *Syn3: A program for inversion of teleseismic body waveforms on microcomputers,* Tech. rep., Air Force Geophys. Lab. Tech. Rep., AFGL-TR-88-0099, Hanscomb Air Force Base, Mass.

McCaffrey, R., Abers, G. & Zwick, P., 1991. *Inversion of Teleseismic Body Waves, Digital Seismogram Analysis and Waveform Inversion,* IASPEI Software Library, Vol. 3, chapter 3, Seismol. Soc. of America, El Cerrito, CA.

McClusky, S. *et al.*, 2000. Global Positioning System constraints on plate kinematics and dynamics in the eastern Mediterranean and Caucasus, *J. geophys. Res.: Solid Earth,* **105**(B3), 5695–5719.

McKenzie, D., 1972. Active tectonics of the Mediterranean region, *Geophys. J. Int.,* **30**(2), 109–185.

McKenzie, D., 1978. Active tectonics of the Alpine—Himalayan belt: the Aegean Sea and surrounding regions, *Geophys. J. Int.,* **55**(1), 217–254.

McKenzie, D. & Jackson, J., 1983. The relationship between strain rates, crustal thickening, palaeomagnetism, finite strain and fault movements within a deforming zone, *Earth planet. Sci. Lett.,* **65**(1), 182–202.

McKenzie, D. & Jackson, J., 1986. A block model of distributed deformation by faulting, *J. geol. Soc.,* **143**(2), 349–353.

McKenzie, D. & Jackson, J., 2012. Tsunami earthquake generation by the release of gravitational potential energy, *Earth planet. Sci. Lett.,* **345-348,** 1–8.

Mercier, J. L., Sorel, D., Vergely, P. & Simeakis, K., 1989. Extensional tectonic regimes in the aegean basins during the cenozoic, *Basin Res.,* **2**(1), 49–71.

Mercier, J. L., Sebrier, M., Lavenu, A., Cabrera, J., Bellier, O., Dumont, J.-F. & Machrare, J., 1992. Changes in the tectonic regime above a subduction zone of Andean Type: the Andes of Peru and Bolivia during the Pliocene-Pleistocene, *J. geophys. Res.: Solid Earth,* **97**(B8), 11945–11982.

Metaxas, A., Karageorgiou, D., Varvarousis, G., Kotis, T., Ploumidis, M. & Papanikolaou, G., 2007. Geological evolution–stratigraphy of Florina, Ptolemaida, Kozani and Sarantaporo graben, *Bull. geol. Soc. Greece,* **40**(1), 161–172.

Métois, M. *et al.*, 2015. Insights on continental collisional processes from GPS data: dynamics of the peri-Adriatic belts, *J. geophys. Res.: Solid Earth,* **120**(12), 8701–8719.

Molnar, P. & Lyon-Caen, H., 1988. Some simple physical aspects of the support, structure, and evolution of mountain belts, *Geol. Soc. Am. Spec. Papers,* **218,** 179–208.

Molnar, P. & Lyon-Caen, H., 1989. Fault plane solutions of earthquakes and active tectonics of the Tibetan Plateau and its margins, *Geophys. J. Int.,* **99**(1), 123–153.

Mortera-Gutiarrez, C. A., Scholl, D. W. & Carlson, R. L., 2003. Fault trends on the seaward slope of the Aleutian Trench: implications for a laterally changing stress field tied to a westward increase in oblique convergence, *J. geophys. Res.: Solid Earth,* **108**(B10), doi:10.1029/2001JB001433.

Papadopoulos, G. A., Agalos, A., Carydis, P., Lekkas, E., Mavroulis, S. & Triantafyllou, I., 2020. The 26 November 2019 Mw 6.4 Albania Destructive Earthquake, *Seismol. Res. Lett.,* **91**(6), 3129–3138.

Pavlides, S. & Mountrakis, D., 1986. Neotectonics of the Florina-Vegoritis-Ptolemais Neogene Basin (NW Greece): an example of extensional tectonics of the greater Aegean area, *Ann. Géol. Pays Hell.,* **33**(11), 311–327.

Pavlides, S. & Mountrakis, D., 1987. Extensional tectonics of northwestern Macedonia, Greece, since the late Miocene, *J. Struct. Geol.,* **9**(4), 385–392.

Reicherter, K., Hoffmann, N., Lindhorst, K., Krastel, S., Fernández-Steeger, T., Grützner, C. & Wiatr, T., 2011. Active basins and neotectonics: morphotectonics of the Lake Ohrid Basin (FYROM and Albania), *Zeitschrift der Deutschen Gesellschaft für Geowissenschaften,* **162**(2), 217–234.

Reilinger, R., McClusky, S., Paradissis, D., Ergintav, S. & Vernant, P., 2010. Geodetic constraints on the tectonic evolution of the Aegean region and strain accumulation along the Hellenic subduction zone, *Tectonophysics,* **488**(1), 22–30.

Roure, F., Nazaj, S., Mushka, K., Fili, I., Cadet, J.-P. & Bonneau, M., 2004. Kinematic evolution and petroleum systems – an appraisal of the outer albanides, *Thrust Tectonics and Hydrocarbon Systems,* Vol. **82,** pp. 474—493, Tulsa, AAPG Memoir.

Sandwell, D. T., Müller, R. D., Smith, W. H. F., Garcia, E. & Francis, R., 2014. New global marine gravity model from CryoSat-2 and Jason-1 reveals buried tectonic structure, *Science,* **346**(6205), 65–67.

Schmitz, B., Biermanns, P., Hinsch, R., Daković, M., Onuzi, K., Reicherter, K. & Ustaszewski, K., 2020. Ongoing shortening in the dinarides fold-and-thrust belt: A new structural model of the 1979 (mw 7.1) Montenegro earthquake epicentral region, *J. Struct. Geol.,* **141,** 104192, doi:10.1016/j.jsg.2020.104192.

Shaw, B. & Jackson, J., 2010. Earthquake mechanisms and active tectonics of the Hellenic subduction zone, *Geophys. J. Int.,* **181**(2), 966–984.

Shaw, B. *et al.*, 2008. Eastern Mediterranean tectonics and tsunami hazard inferred from the AD 365 earthquake, *Nat. Geosci.,* **1**(4), 268–276.

Shen, Z.-K., Wang, M., Zeng, Y. & Wang, F., 2015. Strain determination using spatially discrete geodetic data, *Bull. seism. Soc. Am.,* **105**(4), 2117–2127.

Sodoudi, F. *et al.*, 2006. Lithospheric structure of the aegean obtained from p and s receiver functions, *J. geophys. Res.: Solid Earth,* **111**(B12), doi:10.1029/2005JB003932.

Speranza, F., Islami, I., Kissel, C. & Hyseni, A., 1995. Paleomagnetic evidence for Cenozoic clockwise rotation of the external Albanides, *Earth planet. Sci. Lett.,* **129**(1), 121–134.

Steenbrink, J., Hilgen, F., Krijgsman, W., Wijbrans, J. & Meulenkamp, J., 2006. Late Miocene to Early Pliocene depositional history of the intramontane Florina–Ptolemais–Servia Basin, NW Greece: interplay between

orbital forcing and tectonics, *Palaeog. Palaeoclimat. Palaeoecol.,* **238**(1), 151–178.
Sulstarova, E. & Koçiaj, S., 1980. The Dibra (Albania) earthquake of November 30, 1967, *Tectonophysics,* **67**(3), 333–343.
Talebian, M. & Jackson, J., 2004. A reappraisal of earthquake focal mechanisms and active shortening in the Zagros mountains of Iran, *Geophys. J. Int.,* **156**(3), 506–526.
Taymaz, T., Jackson, J. & Westaway, R., 1990. Earthquake mechanisms in the Hellenic Trench near Crete, *Geophys. J. Int.,* **102**(3), 695–731.
Taymaz, T., Jackson, J. & McKenzie, D., 1991. Active tectonics of the north and central Aegean Sea, *Geophys. J. Int.,* **106**(2), 433–490.
Thatcher, W., 2009. How the continents deform: the evidence from tectonic geodesy, *Annu. Rev. Earth Planet. Sci.,* **37,** 237–262.
Tolomei, C., Caputo, R., Polcari, M., Famiglietti, N. A., Maggini, M. & Stramondo, S., 2021. The use of interferometric synthetic aperture radar for isolating the contribution of major shocks: the case of the March 2021 Thessaly, Greece, Seismic Sequence, *Geosciences,* **11**(5), doi:10.3390/geosciences11050191.
Tozer, B., Sandwell, D. T., Smith, W. H. F., Olson, C., Beale, J. R. & Wessel, P., 2019. Global bathymetry and topography at 15 arc sec: Srtm15+, *Earth Space Sci.,* **6**(10), 1847–1864.
Tucker, G. E., McCoy, S. W., Whittaker, A. C., Roberts, G. P., Lancaster, S. T. & Phillips, R., 2011. Geomorphic significance of postglacial bedrock scarps on normal-fault footwalls, *J. geophys. Res.: Earth Surface,* **116**(F1), doi:10.1029/2010JF001861.
Valkaniotis, S. *et al.*, 2020. The Mw = 5.6 Kanallaki Earthquake of 21 March 2020 in West Epirus, Greece: reverse fault model from InSAR data and seismotectonic implications for Apulia-Eurasia Collision, *Geosciences,* **10**(11), doi:10.3390/geosciences10110454.
van Vugt, N., Steenbrink, J., Langereis, C., Hilgen, F. & Meulenkamp, J., 1998. Magnetostratigraphy-based astronomical tuning of the early Pliocene lacustrine sediments of Ptolemais (NW Greece) and bed-to-bed correlation with the marine record, *Earth planet. Sci. Lett.,* **164**(3), 535–551.
Velaj, T., 2012. Thrust tectonics and the role of evaporites in the Ionian zone of the Albanides, *Nafta,* **63**(7-8), 236–242.
Vittori, E., Blumetti, A. M., Comerci, V., DiÂ Manna, P., Piccardi, L., Gega, D. & Hoxha, I., 2020. Geological effects and tectonic environment of the 26 November 2019, Mw 6.4 Durres earthquake (Albania), *Geophys. J. Int.,* **225**(2), 1174–1191.
Wallace, R. E., 1987. Grouping and migration of surface faulting and variations in slip rates on faults in the Great Basin province, *Bull. seism. Soc. Am.,* **77**(3), 868–876.
Wessel, P., Luis, J. F., Uieda, L., Scharroo, R., Wobbe, F., Smith, W. H. F. & Tian, D., 2019. The generic mapping tools version 6, *Geochem. Geophys. Geosyst.,* **20**(11), 5556–5564.
Wimpenny, S., Copley, A., Benavente, C. & Aguirre, E., 2018. Extension and dynamics of the Andes inferred from the 2016 Parina (Huarichancara) earthquake, *J. geophys. Res.: Solid Earth,* **123,** 8198–8228.
Wimpenny, S., Benavente, C., Copley, A., Garcia, B., Rosell, L., O'Kane, A. & Aguirre, E., 2020. Observations and dynamical implications of active normal faulting in South Peru, *Geophys. J. Int.,* **222**(1), 27–53.
Xhomo, A., Nazaj, S., Nakuci, V., Yzeiraj, D., Lula, F. & Sadushi, P., 2002. *Geological map of albania (1:200.000),* Tech. rep., Ministry of Industry and Energy, Ministry of Education and Science, Albanien Geological Survey, AlpPetrol, Polytechnical University of Tirana.
Yielding, G., Jackson, J., King, G., Sinvhal, H., Vita-Finzi, C. & Wood, R., 1981. Relations between surface deformation, fault geometry, seismicity, and rupture characteristics during the El Asnam (Algeria) earthquake of 10 October 1980, *Earth planet. Sci. Lett.,* **56,** 287–304.
Zhu, L., Mitchell, B. J., Akyol, N., Cemen, I. & Kekovali, K., 2006. Crustal thickness variations in the aegean region and implications for the extension of continental crust, *J. geophys. Res.: Solid Earth,* **111**(B1), doi:10.1029/2005JB003770.
Zwick, P., McCaffrey, R. & Abers, C., 1995. *Mt5 Program, in Bibliographic References and BSSA Database, IASPEI Software Library,* Vol. **4,** Seismol. Soc. of America, El Cerrito, CA.

SUPPORTING INFORMATION

Supplementary data are available at *GJI* online.

Figure S1. Minimum misfit solution for the earthquake of 2002 April 24.
Figure S2. Minimum misfit solution for the earthquake of 2009 May 24.
Figure S3. Minimum misfit solution for the earthquake of 2009 September 06.
Figure S4. Minimum misfit solution for the earthquake of 2013 August 07.
Figure S5. Minimum misfit solution for the earthquake of 2016 October 15.
Figure S6. Minimum misfit solution for the earthquake of 2018 July 04.
Figure S7. Minimum misfit solution for the thrust faulting earthquake of 2019 June 01.
Figure S8. Minimum misfit solution for the thrust faulting earthquake of 2019 October 19 near Durres in Albania.
Figure S9. Minimum misfit solution for the thrust faulting earthquake of 2019 November 26 near Durres in Albania.
Figure S10. Minimum misfit solution for the main aftershock of the thrust faulting earthquake of 2019 November 26 near Durres in Albania.
Figure S11. Minimum misfit solution for the thrust faulting earthquake of 2020 March 21 near Paramythia in Greece.
Figure S12. Minimum misfit solution for the thrust faulting earthquake of 2021 March 03 near Tirnavos in Greece.
Figure S13. Minimum misfit solution for the normal faulting earthquake of 2022 January 09 near Florina in Greece. The strike, dip and rake have been constrained to the global CMT solution (Table S3) and only depth and source time function (STF) have been inverted. The station SJG, marked with an asterisk, in the figure, was not used in the inversion. The WKBJ forward modelling (bottom) confirms the 15 km depth.
Table S1. Earthquake source parameters determined by body wave modelling (this study).
Table S2. Earthquake source parameters determined by body wave modelling from previous studies. Ref. 1: Taymaz *et al.* (1991); ref. 2: Hatzfeld *et al.* (1996); ref. 3: Baker *et al.* (1997); ref. 4: Bernard *et al.* (1997); ref. 5: Hatzfeld *et al.* (1997); ref. 6: Louvari *et al.* (2001); ref .7: Copley *et al.* (2009); ref. 8: Boait and ref. 9: Louvari and Kiratzi (2001).
Table S3. Global CMT events (http://www.globalcmt.org. We calculate the percentage of double-couple component following Jackson et al. (2002) as $\gamma = 100\{1 - [(2|\lambda_2| \times 1.5)/(|\lambda_1| + |\lambda_3|)]\}$., where λ_1, λ_2, λ_3 are the minimum, intermediate and largest eigenvalues of the seismic moment tensor.
Table S4. First motion solutions. Ref. 1: McKenzie (1972) and ref. 2: Anderson and Jackson (1987).
Table S5. Regional CMT; http://rcmt2.bo.ingv.it/Italydataset.html. WKBJ is the depth estimated by modelling the *pP*, *Sp* depth phases with the WKBJ3 software (Chapman 1978).

Please note: Oxford University Press is not responsible for the content or functionality of any supporting materials supplied by the authors. Any queries (other than missing material) should be directed to the corresponding author for the paper.